# JMJD3 activated hyaluronan synthesis drives muscle regeneration in an inflammatory environment

Kiran Nakka, Sarah Hachmer, Zeinab Mokhtari, Radmila Kovac, Hina Bandukwala, Clara Bernard, Yuefeng Li, Guojia Xie, Chengyu Liu, Magid Fallahi, et al.

# JMJD3 activated hyaluronan synthesis drives muscle regeneration in an inflammatory environment

**Short Title:** JMJD3 primes stem cells for inflammation

**One-Sentence Summary:** JMJD3 initiates muscle repair by removing H3K27me3 marks at genes needed to dampen inflammatory block to stem cell function.

Kiran Nakka[1,2], Sarah Hachmer[1,2,†], Zeinab Mokhtari[1,2,†], Radmila Kovac[1,2], Hina Bandukwala[1], Clara Bernard[5], Yuefeng Li[1,2], Guojia Xie[3], Chengyu Liu[4], Magid Fallahi[1], Lynn A. Megeney[1,2], Julien Gondin[5], Bénédicte Chazaud[5], Marjorie Brand[1,2,6], Xiaohui Zha[1,7], Kai Ge[3], F. Jeffrey Dilworth[1,2,6*]

**Affiliations:**

[1]Sprott Center for Stem Cell Research, Regenerative Medicine Program, Ottawa Hospital Research Institute; Ottawa, ON, Canada, K1H 8L6.

[2]Department of Cellular and Molecular Medicine, University of Ottawa; Ottawa, ON, Canada.

[3]National Institute of Diabetes & Digestive & Kidney Diseases, National Institutes of Health; Bethesda, MD, USA.

[4]Transgenic Core, National Heart Lung and Blood Institute, National Institutes of Health; Bethesda, MD, USA.

[5]Institut NeuroMyoGène, Unité Physiopathologie et Génétique du Neurone et du Muscle, Université Claude Bernard Lyon 1, CNRS 5261, INSERM U1315, Université de Lyon, Lyon, France.

[6]LIFE Research Institute, University of Ottawa; Ottawa, ON, Canada.

[7]Department of Biochemistry, Microbiology, and Immunology, University of Ottawa; Ottawa, ON, Canada.

[†]Authors Contributed Equally

*Corresponding author. Email: jdilworth@ohri.ca

Manuscript Length: 4168 words

Figures: 4

References: 36

**Abstract:**

**Muscle stem cells (MuSC) reside in a specialized niche that ensures their regenerative capacity. While we know innate immune cells infiltrate the niche in response to injury, it remains unclear how MuSCs adapt to this altered environment for initiating repair. Here, we demonstrate that inflammatory cytokine signaling from the regenerative niche impairs the ability of quiescent MuSCs to re-enter cell cycle. The H3K27-demethylase JMJD3, but not UTX, allows MuSCs to overcome inhibitory inflammation signaling by removing H3K27me3 marks at the *Has2* locus to initiate production of hyaluronic acid, which in turn establishes an extracellular matrix competent for integrating signals that direct MuSCs to exit quiescence. Thus, JMJD3 driven hyaluronic acid synthesis plays a pro-regenerative role allowing MuSC adaptation to inflammation and initiation of muscle repair.**

Muscle stem cells (MuSCs) provide skeletal muscle with a remarkable capacity for regeneration after tissue damage (*1*). After sterile injury in mice, regenerative process is initiated by necrosis of the damaged myofibers and release of myokines that instruct the recruitment of a variety of tissue resident and infiltrating cell-types that coordinate muscle repair (*2*). Approximately 24-40h after injury, when the clearing of necrotic fibers is well underway, assembly of the regenerative milieu signals the resident MuSCs to exit quiescence (thus activate) and expand their population before undergoing terminal differentiation, leading ultimately to new myofiber formation (*3*). Tight control of signal integration from the regenerative milieu ensures a sufficient expansion of the muscle progenitor population to mediate both myofiber repair and stem cell niche repopulation (*4, 5*). Recent work has implicated a population of infiltrating macrophages in the establishment of a transient niche for MuSCs that is required for re-entry of quiescent stem cells into cell cycle (*6*). However, how MuSCs adapt to this altered local environment and initiate the regenerative process remains unknown.

Isolation of quiescent MuSCs from their niche in healthy muscle results in the rapid activation of a stress response that is accompanied by alteration of the epigenetic landscape (*7, 8*). This suggests that epigenetic enzymes could contribute to the activation of MuSC in the regenerative milieu. Among the different epigenetic changes induced by injury, global levels of trimethylated histone H3 lysine 27 (H3K27me3) are reduced in MuSCs as they transition from the quiescent to the proliferative state (*9*). The removal of H3K27me3 marks is mediated by the KDM6 family of H3K27-demethylases which includes the JMJD3 and UTX proteins (*10, 11*). While H3K27me3 marks are tightly linked to transcriptional repression (*12, 13*), the importance of active H3K27me3 removal to tissue development and repair has been called into question by developmental studies in which mouse embryos lacking both JMJD3 and UTX survive to term (*14*). However, regeneration after injury could be distinct from tissue development, as it inevitably begins in an inflammatory environment. Here we set out to examine the importance of H3K27-demethylation, particularly the individual roles of JMJD3 and UTX, in the adaptation of MuSCs to regenerative milieu of injured muscle.

MuSCs express both UTX and JMJD3 (Fig. S1). To determine how each H3K27-demethylase enzyme contributes to muscle regeneration, we generated MuSC-specific knockouts of UTX ($UTX^{scKO}$) or JMJD3 ($JMJD3^{scKO}$) in mice (Fig. S2A-C). Upon acute cardiotoxin (CTX) injury of the tibialis anterior (TA) muscle, both the $UTX^{scKO}$ and the $JMJD3^{scKO}$ mice showed impaired myofiber regeneration, demonstrating that KDM6 proteins play non-redundant roles in MuSC-mediated muscle regeneration (Fig. 1A, S3). To investigate the specific roles played by UTX and JMJD3 in regeneration, we performed scRNA-Seq analysis on purified MuSCs isolated at 40h post-injury, a time point at which MuSCs usually enter cell cycle (*15*). Plotting individual cells across a pseudotime trajectory, we observed that UTX-null MuSCs efficiently entered cell cycle and accumulated in cluster 3 which is enriched for a MuSC proliferation gene signature (Fig. 1B-C, S4). In contrast, JMJD3-null MuSCs showed a delayed progression along the trajectory with an overrepresentation of cells present in cluster 0, a cluster enriched for an immediate-early MuSC activation gene signature (Fig. 1B-C, S4). Additionally, we observed that MuSCs from $JMJD3^{scKO}$ mice were underrepresented in clusters associated with proliferation (Fig. 1C). These findings suggested that JMJD3 might be required for the efficient transition of MuSCs from a quiescent to proliferating state. To explore a role for JMJD3 in cell cycle re-entry, mice were given an *i.p.* injection of the thymidine analog EdU at 28h post-injury, and examined for the percentage of MuSCs that had transitioned into the cell cycle at 40h post-injury. While MuSCs from WT or $UTX^{scKO}$ mice efficiently progressed into cell cycle, MuSCs from $JMJD3^{scKO}$ mice were impaired in their progression through S-phase (Fig. 1D). Thus, JMJD3, but not UTX, is required for efficient

activation of MuSCs in the regenerative milieu. At the same time, we observed that UTX, but not JMJD3, is required for MuSCs to exit cell cycle and undergo terminal differentiation (Fig. S5A) (*16*), while neither H3K27 demethylase was required for proliferation of the MuSCs population (Fig. S5B). Thus, JMJD3 and UTX play non-redundant roles in MuSCs, where they act at distinct stages of muscle regeneration.

To determine whether JMJD3 was acting through its enzymatic activity to mediate MuSC activation, an enzyme-dead JMJD3 knock-in ($JMJD3^{scDD}$) mouse was generated using CRISPR-mediated mutagenesis of the endogenous locus (Fig. S6A-B). Similar to JMJD3-null cells, $JMJD3^{scDD}$ MuSCs that lacked demethylase activity showed inefficient re-entry into cell cycle following injury (Fig. 1D). This defect in MuSC activation impaired the ability of $JMJD3^{scDD}$ mice to repair damaged muscle after CTX injury (Fig. S6C-D). Thus, JMJD3 acts through its enzymatic activity to facilitate the exit of quiescence for MuSCs after muscle injury.

To study the mechanism through which H3K27-demethylation contributes to the activation process, MuSCs from WT, $UTX^{scKO}$, $JMJD3^{scKO}$ and $JMJD3^{scDD}$ mice were purified from healthy muscle for characterization *ex vivo*. To our surprise, when allowed to activate *ex vivo*, purified (or myofiber-associated) MuSCs from $JMJD3^{scKO}$ and $JMJD3^{scDD}$ mice no longer displayed a defect in activation, and were able to re-enter cell cycle with an efficiency similar to that displayed by MuSC from WT and $UTX^{scKO}$ mice (Fig. 2A, S7). Thus, JMJD3 (or its demethylase activity) were not necessary for entry into cell cycle if the MuSCs were isolated from an uninjured muscle. These findings suggest that JMJD3 may coordinate MuSC activation upon inflammatory signals from the regenerative milieu. To test this possibility, we injured the TA muscle in one leg of the mouse, and then waited 30h before measuring the ability of purified MuSC from the contralateral leg to re-enter cell cycle. Analysis of MuSCs isolated from uninjured muscles of $JMJD3^{scKO}$ and $JMJD3^{scDD}$ mice showed impaired cell cycle re-entry (compared to WT or $UTX^{scKO}$ MuSCs) if the mouse was recovering from an injury to the contralateral leg (Fig. 2A, S8). This suggests that a signaling molecule(s) from the injured muscle could inhibit activation of MuSCs, and that JMJD3 is required to overcome this inhibition. We note this inhibitory signal from the injured muscle did not need to be sustained to impair activation since purified JMJD3-null MuSCs from the contralateral leg continued to show delayed cell cycle re-entry when activation was measured *ex vivo* (Fig. 2A, S8). Interestingly, we observe that this inhibitory signal from injured muscle environment is not specific to JMJD3-null mice since a soluble extract (dMusEx - prepared using CTX-injured muscle from WT mice) added to cultured myofibers could also inhibit cell cycle re-entry of JMJD3-mutant MuSCs, but not WT or $UTX^{scKO}$ MuSCs (Fig. 2B, S9). Similarly, a soluble extract (MdxMusEx) made from dystrophic muscle also impaired activation of JMJD3-null MuSCs (Fig 2B), showing that MuSC activation in chronic muscle conditions also requires JMJD3. Taken together, these results show that JMJD3 facilitates MuSC activation in a non-cell autonomous manner by overcoming an inhibition signal originating in the regenerative niche. However, the mechanism by which JMJD3 acts to allow MuSCs to integrate activation signaling from the regenerative milieu is unclear.

To determine how JMJD3 permits MuSCs to overcome inhibitory signals from the regenerative niche, we searched for target genes expressed in MuSCs isolated 30h after CTX injury (Fig. 3, S10, and Table S1). Differential expression analysis showed that JMJD3 is required for the expression of 325 genes in activating MuSCs (Fig. 3A). While UTX also activates expression of 317 genes, we observed only a small overlap with those regulated by JMJD3. Consistent with their roles as H3K27-demethylases, ablation of either UTX or JMJD3 resulted in a generalized increase in H3K27me3 enrichment at the promoters of their respective target genes (Fig. 3B). Gene ontology (GO) analysis showed that UTX is required for the expression of genes associated with

development (Fig. S10A-B) while the loss of JMJD3 resulted in decreased expression of genes associated with migration and cell cycle (Fig. 3C, S10C). Thus, JMJD3 and UTX function as transcriptional regulators at distinct sets of genes in MuSCs.

To identify direct JMJD3 target genes that could mediate the communication between MuSCs and the regenerative environment, we assembled a gene list based on three properties: 1) expression was decreased in JMJD3$^{scKO}$ MuSCs but not UTX$^{scKO}$ MuSCs; 2) JMJD3 binds within 2500 bp of the promoter; and 3) accumulation of H3K27me3 near the gene upon ablation of JMJD3. Among the 41 genes meeting these criteria (Table S1), we identified several genes associated with remodeling the extracellular matrix (ECM). Amongst these genes, *Has2* (Fig. 3D) encodes the key enzyme involved in the synthesis of hyaluronic acid (HA), a linear glycosaminoglycan polymer that contributes to the ECM to alter its rigidity (*17*) while providing a rheostat for various signaling pathways (*18*). Furthermore, HA is used therapeutically to modulate inflammation in a broad range of tissues (*19*), including muscle (*20*), suggesting it may be a candidate for mediating the effects of JMJD3 on MuSC activation.

Analyzing published datasets (*21, 22*), we observed that *Has2* is not expressed in quiescent MuSCs but is upregulated during MuSC activation in uninjured muscle (Fig. S11A) or in regenerating muscle after freeze injury (Fig. S11B). Consistent with this, we observe that HA is present in the myofiber ECM of regenerating (40h post-injury) muscle and envelops the activated MuSCs within the niche of WT or dystrophic mice (Fig. 4A, S12A-D). Remarkably, the ECM of MuSCs in regenerating muscle from JMJD3$^{scKO}$ and JMJD3$^{scDD}$ mice is devoid of detectible HA (Fig. 4A, S12A-B). This dynamic incorporation of HA into the ECM of MuSCs suggests it could play an important role in muscle regeneration. To test this possibility, we inhibited the production of HA in WT mice through systemic delivery of the small molecule inhibitor 4-methylumbelliferone (4-MU) (*23*) during muscle regeneration. Histological analysis showed impaired MuSC-mediated regeneration when HA synthesis was inhibited by 4-MU (Fig. S13A-B). This impaired muscle regeneration in the absence of HA synthesis results from delayed MuSC activation as assessed by EdU incorporation (Fig. S13C). This shows that MuSC that express JMJD3 are impaired in their exit of quiescence *in vivo* when they fail to make HA. Interestingly, purified WT MuSCs (from uninjured mice) were able to efficiently exit quiescence in the presence of the 4-MU, while MuSCs incubated with an extract from damaged muscle (dMusEx) were sensitive to 4-MU treatment and showed impaired cell cycle re-entry (Fig. 4B). Thus, MuSCs require HA synthesis to coordinate efficient exit of quiescence in a regenerative niche environment.

Having established that HA synthesis is required for activation of WT MuSCs, we next asked whether an exogenous HA treatment would rescue the activation defect in JMJD3-null MuSCs (Fig. 4C, S14-S16). Examining myofiber explants isolated from mice with a prior injury to the contralateral leg, we observed reduced activation of JMJD3-null MuSCs that could be rescued by supplementation with exogenous high molecular weight HA (Fig. S14). Similarly, HA treatment could rescue the damaged muscle extract induced-block in activation observed in MuSCs from JMJD3$^{scKO}$ and JMJD3$^{scDD}$ mice (Fig. 4C, S15-S16). Thus, incorporation of HA into the ECM is sufficient to prepare MuSCs to integrate signals from the regenerative milieu that initiate cell cycle re-entry.

Finally, we explored the nature of the niche-derived signals that were responsible for impeding MuSC activation in the absence of JMJD3. Gene Set Enrichment Analysis (GSEA) using the Hallmark Molecular Signature Database (*24*) showed strong correlation between transcripts up-regulated in MuSCs from JMJD3$^{scKO}$ mice and the cellular responses to various inflammatory cytokines (Figure S17A, Table S1). Concurrent with this elevated response to inflammation in

MuSCs, we observed a 2-fold increase in the infiltration of hematopoietic ($CD45^+$) cells into the regenerating $JMJD3^{scKO}$ muscle (Fig S17B). The most significant cytokine response observed in genes upregulated in JMJD3-null MuSCs was towards the inflammatory peptides IFNγ (Fig. S17A, S17C), a cytokine that promotes proliferation but has pleiotropic effects in muscle (*25*). Elevated levels of IFNγ protein could be detected in muscle from injured or dystrophic muscle, as well as an uninjured muscle when isolated from a mouse after previous injury to the contralateral leg (Fig S17D). In addition, we observed increased expression of key IFNγ target genes in the contralateral leg of mice of previously injured mice (Fig S17E). Consistent with recent reports showing that elevated IFNγ levels observed in inclusion body myositis leads to impaired MuSC activation (*26*), we observed that exogenous IFNγ prevented the efficient activation of myofiber-associated MuSCs from $JMJD3^{scKO}$ mice (Fig. 4C, S18). Importantly, the inhibitory effects of IFNγ could be rescued by providing exogenous HA (Fig. 4C, S18). Finally, similar impairment to activation could be observed in JMJD3-null MuSCs when treated with IL6, a cytokine that also works through JAK/STAT signaling, but not TNFα which works through NF-κB (Figure S19). The source of the IFNγ and IL6 signals in the regenerating muscle likely derives (at least in part) from macrophages since the expression of both cytokines is observed in $Ly6C^+$ cells purified from muscle 24h after injury (Fig. S20). This suggests that JMJD3-induced HA synthesis contributes to the establishment of an ECM suitable for modulating pleiotropic effects of cytokine signaling. Thus, we propose a model in which the pro-inflammatory cytokines (including IFNγ and IL6) from the regenerative niche provides an inhibitory signal that prevents MuSCs from undergoing an untimely exit of quiescence. To overcome the cytokine-mediated block to stem cell function, MuSC would initiate *Has2* expression in a JMJD3-dependent manner, where incorporation of HA into the remodeled ECM would render the cells competent to receive pro-regenerative signals. While high-molecular weight HA is used clinically to treat inflammation in degenerative conditions, its mode of action remains poorly understood (*27*). Our studies suggest that HA has not only anti-inflammatory effects on injured tissues but also pro-regenerative activity that stimulates stem cell mediated tissue repair.

Here we have shown that the KDM6 family members UTX and JMJD3 are both required for efficient muscle regeneration. Our finding that two epigenetic factors with the same enzymatic activity play distinct, non-redundant roles in muscle regeneration is surprising. Indeed, epigenetic factors with the same enzymatic activity are often thought of as interchangeable, and as being able to compensate for each other functionally. In contrast, our findings clearly establish that UTX promotes expression of developmental genes whereas JMJD3 allows MuSCs to communicate with the regenerative milieu. Thus, this work revealed a previously unappreciated level of specificity in enzyme-mediated epigenetic regulation. It remains to be determined if such exquisite functional specificity is unique to H3K27 demethylases or also exist for other epigenetic enzymes with the same target specificity. Interestingly, during evolution, UTX emerged early in organisms with bilateral symmetry (*28*), while JMJD3 appeared coincidentally with the development of a more complex innate immune system in placental mammals (*28, 29*). Given the importance of JMJD3 to inflammation response in macrophages (*30*), it is tempting to speculate that mammalian MuSCs have evolved to express JMJD3 in order to better coordinate the innate immune response in regenerating muscle. It remains to be determined whether this JMJD3-dependent coordination of somatic stem cell function with injury-induced tissue inflammation is shared with other regenerative cell types.

In summary, our studies have revealed the importance of the epigenetic enzyme JMJD3 in modulating the expression of its target gene Has2, and that the resulting production of HA allows MuSCs to integrate pro-regenerative signaling from the niche during the repair of injured muscle.

## Method Summary

Mice with a MuSC-specific ablation of JMJD3 (JMJD3$^{scKO}$) or UTX (UTX$^{scKO}$) were characterized for their role in muscle regeneration using *in vivo* and *ex vivo* approaches. Repair of cardiotoxin-injured muscles was analyzed using histological and immunofluorescent approaches. Exit of quiescence for MuSCs was measured by EdU-incorporation to mark entry into S-phase of the cell cycle. Genomic and transcriptomic analysis identified targets genes of JMJD3 and UTX. Detailed procedures for all methods are described in the Supplementary Materials.

## References


1. F. Relaix *et al.*, Perspectives on skeletal muscle stem cells. *Nat Commun* **12**, 692 (2021).
2. M. N. Wosczyna, T. A. Rando, A Muscle Stem Cell Support Group: Coordinated Cellular Responses in Muscle Regeneration. *Dev Cell* **46**, 135-143 (2018).
3. P. Sousa-Victor, L. Garcia-Prat, P. Munoz-Canoves, Control of satellite cell function in muscle regeneration and its disruption in ageing. *Nat Rev Mol Cell Biol* **23**, 204-226 (2021).
4. B. Evano, S. Khalilian, G. Le Carrou, G. Almouzni, S. Tajbakhsh, Dynamics of Asymmetric and Symmetric Divisions of Muscle Stem Cells In Vivo and on Artificial Niches. *Cell Rep* **30**, 3195-3206 (2020).
5. D. C. L. Robinson *et al.*, Negative elongation factor regulates muscle progenitor expansion for efficient myofiber repair and stem cell pool repopulation. *Dev Cell* **56**, 1014-1029 (2021).
6. D. Ratnayake *et al.*, Macrophages provide a transient muscle stem cell niche via NAMPT secretion. *Nature* **591**, 281-287 (2021).
7. C. T. J. van Velthoven, A. de Morree, I. M. Egner, J. O. Brett, T. A. Rando, Transcriptional Profiling of Quiescent Muscle Stem Cells In Vivo. *Cell Rep* **21**, 1994-2004 (2017).
8. L. Machado *et al.*, Tissue damage induces a conserved stress response that initiates quiescent muscle stem cell activation. *Cell Stem Cell* **28**, 1125-1135 e1127 (2021).
9. S. Schworer *et al.*, Epigenetic stress responses induce muscle stem-cell ageing by Hoxa9 developmental signals. *Nature* **540**, 428-432 (2016).
10. K. Agger *et al.*, UTX and JMJD3 are histone H3K27 demethylases involved in HOX gene regulation and development. *Nature* **449**, 731-734 (2007).
11. S. Hong *et al.*, Identification of JmjC domain-containing UTX and JMJD3 as histone H3 lysine 27 demethylases. *Proc Natl Acad Sci U S A* **104**, 18439-18444 (2007).
12. R. Cao *et al.*, Role of histone H3 lysine 27 methylation in Polycomb-group silencing. *Science* **298**, 1039-1043 (2002).
13. M. Brand, K. Nakka, J. Zhu, F. J. Dilworth, Polycomb/Trithorax Antagonism: Cellular Memory in Stem Cell Fate and Function. *Cell Stem Cell* **24**, 518-533 (2019).
14. K. B. Shpargel, J. Starmer, D. Yee, M. Pohlers, T. Magnuson, KDM6 demethylase independent loss of histone H3 lysine 27 trimethylation during early embryonic development. *PLoS Genet* **10**, e1004507 (2014).
15. L. Garcia-Prat *et al.*, FoxO maintains a genuine muscle stem-cell quiescent state until geriatric age. *Nat Cell Biol* **22**, 1307-1318 (2020).
16. H. Faralli *et al.*, UTX demethylase activity is required for satellite cell-mediated muscle regeneration. *J Clin Invest* **126**, 1555-1565 (2016).
17. H. Ge, M. Tian, Q. Pei, F. Tan, H. Pei, Extracellular Matrix Stiffness: New Areas Affecting Cell Metabolism. *Front Oncol* **11**, 631991 (2021).

18. E. Pure, R. K. Assoian, Rheostatic signaling by CD44 and hyaluronan. *Cell Signal* **21**, 651-655 (2009).
19. S. Garantziotis, R. C. Savani, Hyaluronan biology: A complex balancing act of structure, function, location and context. *Matrix Biol* **78-79**, 1-10 (2019).
20. S. Davoudi *et al.*, Muscle stem cell intramuscular delivery within hyaluronan methylcellulose improves engraftment efficiency and dispersion. *Biomaterials* **173**, 34-46 (2018).
21. C. A. Aguilar *et al.*, In vivo Monitoring of Transcriptional Dynamics After Lower-Limb Muscle Injury Enables Quantitative Classification of Healing. *Sci Rep* **5**, 13885 (2015).
22. L. Yue, R. Wan, S. Luan, W. Zeng, T. H. Cheung, Dek Modulates Global Intron Retention during Muscle Stem Cells Quiescence Exit. *Dev Cell* **53**, 661-676 e666 (2020).
23. N. Nagy *et al.*, 4-Methylumbelliferyl glucuronide contributes to hyaluronan synthesis inhibition. *J Biol Chem* **294**, 7864-7877 (2019).
24. A. Liberzon *et al.*, The Molecular Signatures Database (MSigDB) hallmark gene set collection. *Cell Syst* **1**, 417-425 (2015).
25. M. Cheng, M. H. Nguyen, G. Fantuzzi, T. J. Koh, Endogenous interferon-gamma is required for efficient skeletal muscle regeneration. *Am J Physiol Cell Physiol* **294**, C1183-1191 (2008).
26. C. Hou *et al.*, Interferon-gamma mediates skeletal muscle lesions through JAK/STAT pathway activation in inclusion body myositis. *BioRxiv* **https://doi.org/10.1101/2021.12.16.472927v1**, (2021).
27. A. Marinho, C. Nunes, S. Reis, Hyaluronic Acid: A Key Ingredient in the Therapy of Inflammation. *Biomolecules* **11**, (2021).
28. M. National Library of Medicine (Bethesda. (2004), vol. 2021 08 12.
29. T. L. Dunwell, J. Paps, P. W. H. Holland, Novel and divergent genes in the evolution of placental mammals. *Proc Biol Sci* **284**, (2017).
30. F. De Santa *et al.*, The histone H3 lysine-27 demethylase Jmjd3 links inflammation to inhibition of polycomb-mediated gene silencing. *Cell* **130**, 1083-1094 (2007).
31. C. Stringer, T. Wang, M. Michaelos, M. Pachitariu, Cellpose: a generalist algorithm for cellular segmentation. *Nat Methods* **18**, 100-106 (2021).
32. A. Benyoucef *et al.*, UTX inhibition as selective epigenetic therapy against TAL1-driven T-cell acute lymphoblastic leukemia. *Genes Dev* **30**, 508-521 (2016).
33. Y. Li *et al.*, Chromatin and transcription factor profiling in rare stem cell populations using CUT&Tag. *STAR Protoc* **2**, 100751 (2021).
34. F. A. Wolf, P. Angerer, F. J. Theis, SCANPY: large-scale single-cell gene expression data analysis. *Genome Biol* **19**, 15 (2018).
35. M. Setty *et al.*, Characterization of cell fate probabilities in single-cell data with Palantir. *Nat Biotechnol* **37**, 451-460 (2019).
36. T. Varga *et al.*, Highly Dynamic Transcriptional Signature of Distinct Macrophage Subsets during Sterile Inflammation, Resolution, and Tissue Repair. *J Immunol* **196**, 4771-4782 (2016).

**Acknowledgements**

We thank Damian Carragher, Vera Gorbunova, Zhihui Zhang, Penney Gilbert, Sadegh Davoudi, Joe Chakkalakal, Romeo Blanc for insightful discussions; Terry Magnuson for JMJD3$^{fl/fl}$ mice; Odile Neyret for CUT&Tag and RNA-Seq library sequencing; Kathy Sheikheleslamy for

scRNA-Seq library sequencing; uOttawa CBIA core for microscope assistance. Fernando Ortiz for FACS assistance; and Lifang Li for technical help.

**Funding:**
Canadian Institutes of Health Research grant FDN-143330 (FJD)
Canadian Institutes of Health Research grant PJT-156120 (LM)
Canadian Institutes of Health Research grant MOP-343603 (MB)
National Institutes of Health Intramural Research Program of NIDDK (KG)

**Author Contributions:**
Conceptualization: KN, FJD
Methodology: GX, CL, KG, MF
Investigation: KN, SH, YL, CB
Formal Analysis: ZM, HB, RK
Visualization: KN, FJD, ZM, HB
Supervision: FJD, KG, MB, XZ, LM, BC, JG
Writing - original draft: FJD, KN
Writing – review and editing: FJD, KN, MB, KG, LM, XZ, BC

**Competing Interests**
The authors declare they have no competing interests.

**Data and materials availability:**
The RNA-seq, scRNA-Seq and CUT&Tag datasets are available at the Gene Expression Omnibus using accession number GSE186833.

**Supplementary Materials**

Materials and Methods

Figs. S1 to S20

References (*31–36*)

Tables S1

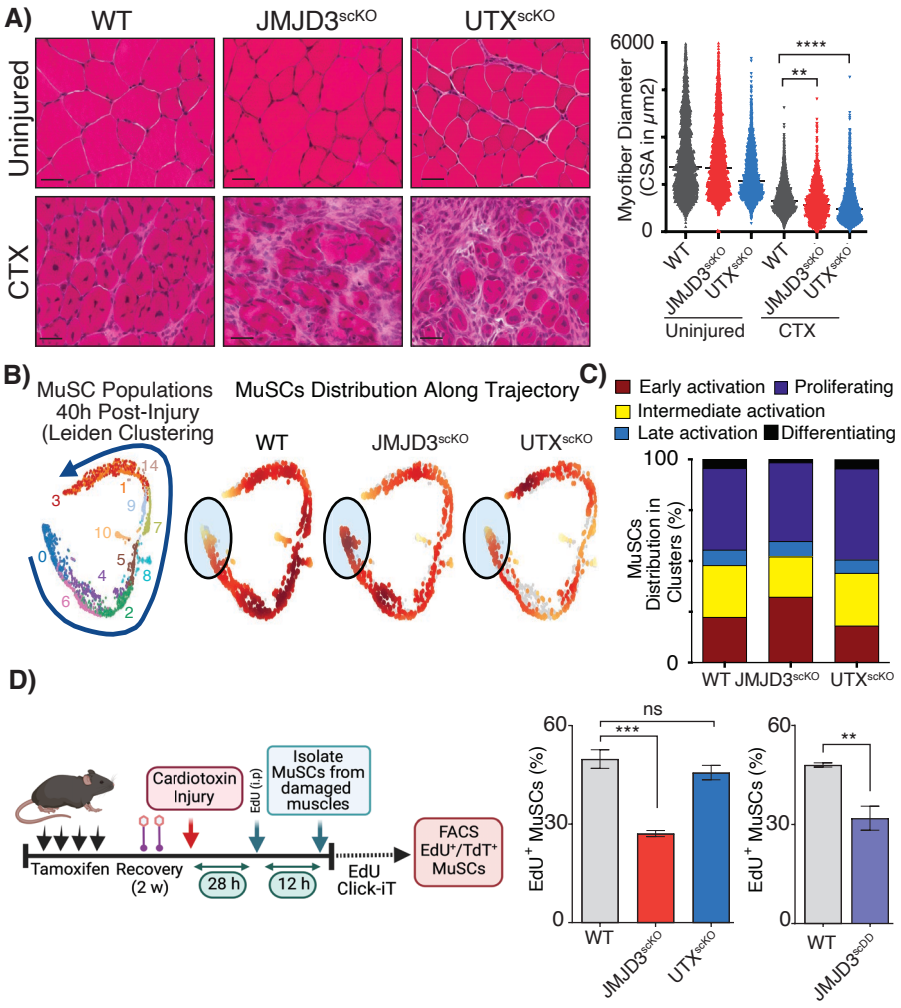


**Figure 1: JMJD3 and UTX play non-redundant roles in muscle regeneration where JMJD3 is required for injury-induced activation of satellite cells. A)** Hematoxylin/Eosin staining of TA muscle cross-sections from WT, JMJD3$^{scKO}$, and UTX$^{scKO}$ mice at 7 days post-injury (CTX). Regeneration was quantified by measuring myofiber diameter. Statistical significance was measure by ANOVA test, n=3. **B)** Clustering and trajectory analysis of combined scRNA-Seq from TdT$^{+}$-purified MuSCs from the WT, JMJD3$^{scKO}$, and UTX$^{scKO}$ mice isolated 30h after muscle injury. **C)** Distribution of MuSCs in clusters representative of different stages of the regenerative process. **D)** Activation of MuSCs was measured by using *in vivo* EdU incorporation to measure first passage of cells through S-phase of the cell cycle between 24 and 40h post injury. FACS analysis measured percentage of MuSCs (TdT+) that were positive for EdU; Statistical significance was measure by unpaired *t*-test, n=3.

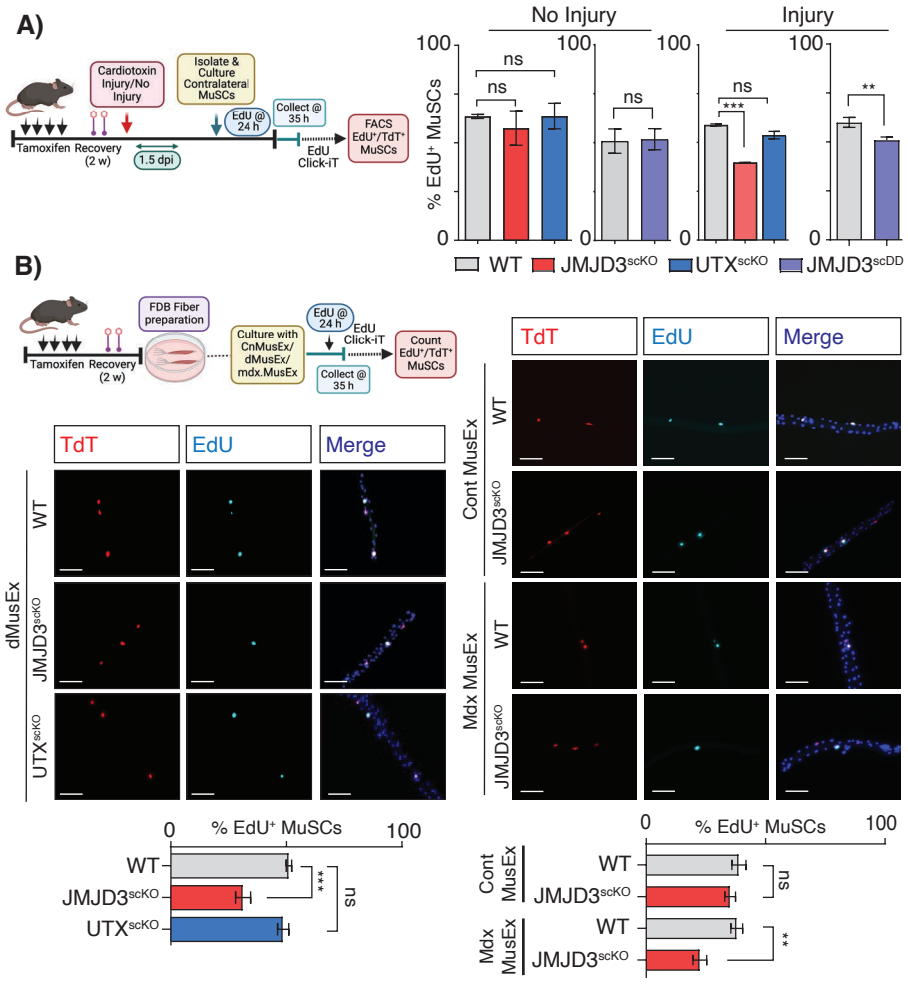


**Figure 2: JMJD3 mediates MuSC activation in a non-cell autonomous manner. A)** Purified MuSCs (TdT+) from uninjured or injured (CTX injury to contralateral leg 36h prior to MuSC isolation from uninjured muscles) mice were assayed *in vitro* using EdU for their first passage of cells through S-phase of the cell cycle between 24 and 40h post injury. FACS analysis measured percentage of MuSCs (TdT+) that were positive for EdU. Statistical significance was measure by unpaired *t*-test, n=3 **B)** *Ex vivo* activation assay where FDB myofiber-associated MuSCs were treated with soluble extracts prepared from uninjured (ContMusEx), injured (dMusEx), or dystrophic (MdxMusEx) muscle. Immunofluorescence analysis measured percentage of MuSCs (TdT+) that were positive for EdU. Statistical significance was measure by unpaired *t*-test, n=3.

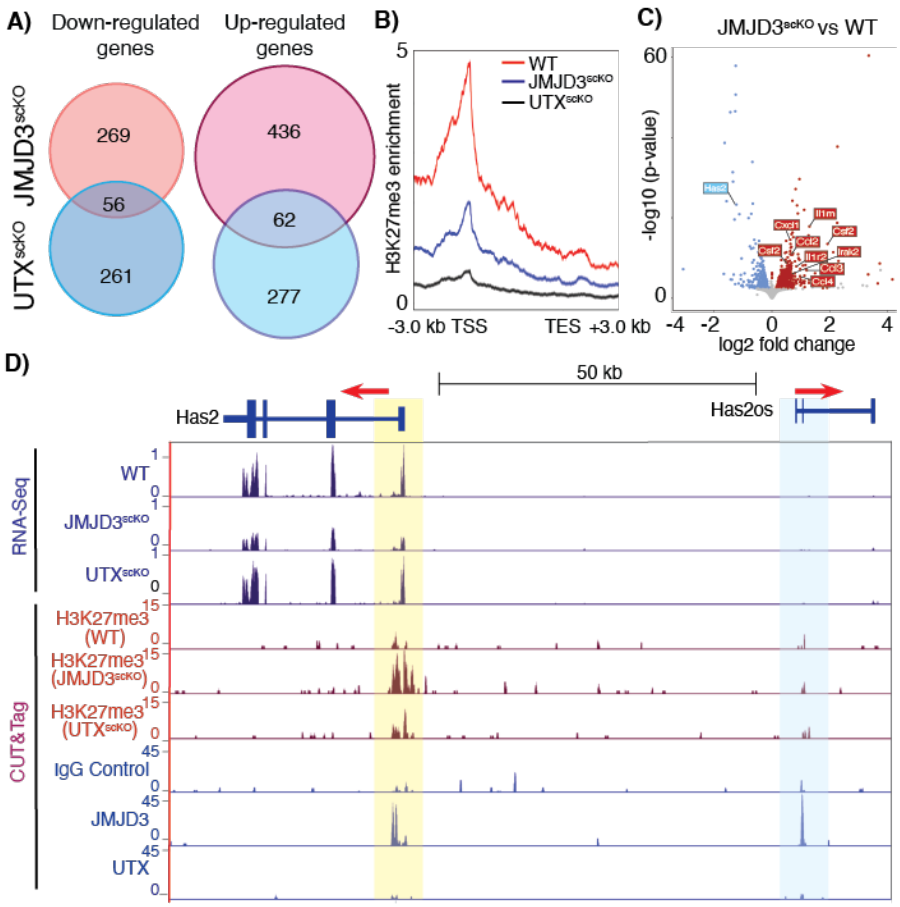


**Figure 3: Has2 is a direct transcriptional target of JMJD3. A)** Venn diagram showing overlap of transcripts that are altered upon loss of UTX or JMJD3 in purified MuSCs at 30h post injury. **B)** Plot of H3K27me3 enrichment across genes that are down-regulated upon loss of JMJD3 or UTX based on CUT&Tag analysis. **C)** Volcano plot showing changes in transcript levels for genes in MuSCs isolated from JMJD3$^{scKO}$ versus WT mice. **D)** UCSC browser track showing the *Has2* locus in MuSCs at 30h post CTX injury (RNA-Seq). Plots include RNA-seq for WT, JMJD3$^{scKO}$, and UTX$^{scKO}$ mice; CUT&Tag analysis showing enrichment of JMJD3, UTX, and H3K27me3.

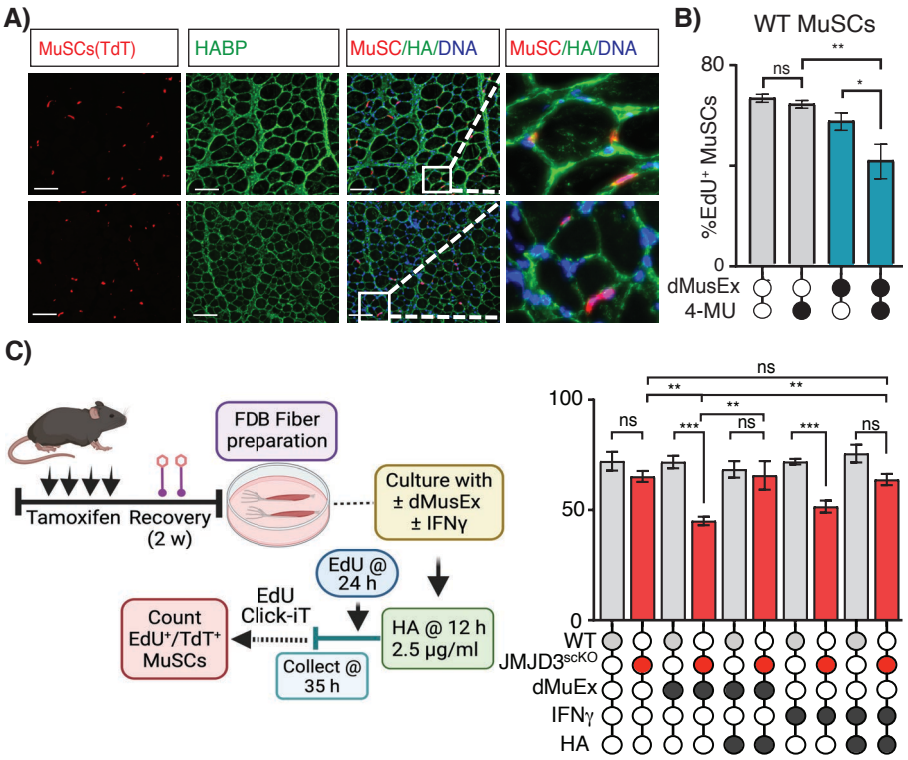


**Figure 4: Hyaluronic acid incorporation into the ECM of MuSCs allows exit of quiescence.** **A)** Immunofluorescence analysis of TA muscle cross-sections at 72h post CTX injury from WT and JMJD3$^{scKO}$ mice. TdT$^{+}$ cells represent MuSCs, HABP identifies HA, and DNA is DAPI staining. **B)** Activation of MuSCs from WT mice was measured in the presence of the HA synthesis inhibitor 4-MU using *in vitro* EdU incorporation. A soluble extract (dMusEx) from damaged WT mouse muscle was added as indicated. FACS analysis measured percentage of MuSCs (TdT+) that were positive for EdU. Statistical significance was measure by unpaired *t*-test, n=3. **C)** *Ex vivo* activation assay of myofiber-associated MuSCs. FDB myofibers isolated form uninjured mice were incubated with either a damaged muscle extract (dMusEx), or recombinant IFNγ protein. HA was added to cultures where indicated. Immunofluorescence analysis measured percentage of MuSCs (TdT+) that were positive for EdU. Statistical significance was measure by unpaired *t*-test, n=3.

Science
AAAS

# Supplementary Materials for

## JMJD3 activated hyaluronan synthesis drives muscle regeneration in an inflammatory environment

Kiran Nakka[1,2], Sarah Hachmer[1,2,†], Zeinab Mokhtari[1,2,†], Radmila Kovac[1,2], Hina Bandukwala[1], Clara Bernard[5], Yuefeng Li[1,2], Guojia Xie[3], Chengyu Liu[4], Magid Fallahi[1], Lynn A. Megeney[1,2], Julien Gondin[5], Bénédicte Chazaud[5], Marjorie Brand[1,2,6], Xiaohui Zha[1,7], Kai Ge[3], F. Jeffrey Dilworth[1,2,6*]

*Correspondence to: jdilworth@ohri.ca

**This PDF file includes:**

Materials and Methods
Supplementary Text
Figs. S1 to S20

**Other Supplementary Material for this manuscript includes the following**

Table S1
MDAR reproducibility checklist

## Materials and Methods

### Generation of mice with muscle stem cell-specific knockouts of UTX or JMJD3

Mouse housing and experimental procedures were performed under the guidelines published by the Canadian Council on the Animal Care (CCAC) and approved by the ethics committee of Animal Care and Veterinary Services at the University of Ottawa under protocols ME3410 and ME3411. Muscle stem cell (MuSC)-specific conditional knockout mice for JMJD3 and UTX were generated by crossing a mouse expressing tamoxifen inducible CreER as a bicistronic transcript from the Pax7 locus (B6.Cg-Pax7$^{tm1(cre/ERT2)\ Gaka}$/J – JAX Strain #017763), with the *Jmjd3*-floxed (B6.129P2(Cg)-Kdm6b$^{tm1Mag}$/Mmnc – Mutant Mouse Resource & Research Center Stock # 037584-UNC) or *Utx*-floxed (B6:129S-Kdm6a$^{tm1.1Kaig}$/J - JAX Strain #024177) mice, respectively. To permit identification of MuSCs that had undergone recombination, Td-tomato reporter was crossed into all lines with using B6.Cg-Gt(ROSA)26Sor$^{tm9(CAG\text{-}Tdtomato)Hze}$/J (JAX Strain #007909) mice. These crosses resulted in the generation of WT (Pax7$^{CreER}$/TdT), JMJD3$^{scKO}$ (Pax7$^{CreER}$/JMJD3$^{fl/fl}$/TdT) and UTX$^{scKO}$ (Pax7$^{CreER}$/UTX$^{fl/fl}$/TdT) mice. Deletion of floxed alleles was achieved by administering daily intra-peritoneal doses of tamoxifen (100 mg/kg body weight) over a period of 4d. The same protocol was used for administrating tamoxifen into the WT mice. In all experiments the mice used were aged between 12 and 18 weeks old.

### Generation of JMJD3 knock-in mice

The JMJD3 H1388A/E1390A knock-in mouse line was generated using CRISPR/Cas9 method while following experimental procedures in accordance with the NIH Guide for the Care and Use of Laboratory Animals and approved by the Animal Care and Use Committee of NIDDK, NIH. An sgRNA targeting genomic locus near JMJD3 H1388A/E1390A (5'-ATTCTCTTGGTGGCCTGCAG -3') was synthesized using Thermo Fisher *in vitro* transcription service. The Histidine to Alanine and Glutamate to Alanine point mutations were introduced using a single-strand Ultramer DNA Oligonucleotide (IDT) as a donor (5' GGTTGTCGCTCCTTGCTCGCCTGCATCAGACCTTCTGTGACGTTCTATCTCCCTCTGC AGGC***GCT***CAA***GCC***AATAACAATTTCTGCTCAGTCAACATCAACATTGGCCCTGGGGA CTGCGAGTGGTTCG -3', in which the inserted mutations are highlighted in italic and bold). To generate the knock-in mouse line, the sgRNA and donor oligonucleotides were co-microinjected

with Cas9 mRNA (Trilink Biotechnologies) into the cytoplasm of zygotes collected from B6D2F1/J mice (JAX Strain #100006). Injected embryos were cultured in M16 medium (Millipore Sigma) overnight in a 37°C incubator with 6% $CO_2$. The next morning, embryos were implanted into the oviducts of pseudopregnant surrogate mothers. Offspring were genotyped by PCR and confirmed by Sanger sequencing. MuSC specific loss of JMJD3-demethylase activity was achieved by crossing heterozygous JMJD3 knock-in mice with JMJD3$^{scKO}$ (Pax7$^{CreER}$/JMJD3$^{KI/fl}$/TdT – hereafter called JMJD3$^{scDD}$) or WT (Pax7$^{CreER}$/JMJD3$^{KI/WT}$/TdT – hereafter called WT) mice. Loss of demethylase activity specifically in MuSCs was achieved upon daily tamoxifen (100 mg/kg body weight) treatment over a period of 4d. The same protocol was used for administrating tamoxifen into the WT mice. Thus, all mice were heterozygous for expression of JMJD3 in MuSCs, where the WT mice expressed a functional JMJD3 protein, and the JMJD3$^{scDD}$ mice expressed a demethylase dead mutant of the protein. All other cell types in the muscle expressed some JMJD3 with demethylase activity. JMJD3scDD mice can be made available via an MTA agreement by contacting Dr. Kai Ge.

**Characterization of injured muscle**

Mice were anaesthetized using isoflurane. Buprenorphine was used an analgesic at a dose of 0.1 mg/kg and was administered sub-cutaneous. For studying muscle regeneration, cardiotoxin was injected to induce acute damage to tibialis anterior muscle with 50 µl of cardiotoxin (10 µM). For experiments where MuSCs were isolated from injured gastrocnemius muscles, 60 µl of cardiotoxin (10 µM) was injected into the larger gastrocnemius muscles.

For histological analysis of regeneration post-injury muscles were harvested from the hind limbs at 7d and 21d post-injury (*16*). Harvested muscles were immersed in Optimal Cutting Temperature (OCT) compound freezing medium (Tissue-Tek), which were subsequently transferred to small tinfoil cups. Muscles were then frozen in isopentane, maintained at subzero temperatures using liquid nitrogen. The muscles were cryosectioned into slices of 10 µm thickness and mounted on to SuperFrost Plus Slides. The slides were subsequently processed or stored in -80°C freezer.

**H&E staining and myofiber diameter measurements**

For Hematoxylin and Eosin staining, the slides were thawed to room temperature and then were incubated in Mayer's hematoxylin solution (Sigma-Aldrich, Cat#MHS80-2.5L) for 5 min. Slides were then rinsed in tap water for 10 sec and then transferred to solution containing 160 mM of Lithium Carbonate (Sigma-Aldrich) for 5 min. Slides were then counterstained in an Eosin bath for 2-3 minutes, before rinsing with tap water. Slides were sequentially soaked for 1 min in 70% ethanol and then 100% ethanol. Finally, the slides were soaked in xylene for 1 min and allowed to dry before they were mounted with coverslips using xylene mounting media. After imaging on a Zeiss Axioscan Z1 microscope, the muscle regeneration was assessed by measuring the cross-sectional area of the centrally located regenerated myofibers. Myofiber cross-section H&E images were segmented by Cellpose 1.0 using the GUI (*31*). Fiber area was measured using the ImageJ plugin, LabelsToRois, by importing the resulting segmentation and the corresponding original images. ROIs were eroded 0-4 pixels after visual inspection.

**Isolation of MuSCs from mice**

MuSCs were isolated from tibialis anterior (TA) and gastrocnemius (Gastroc) muscles of hind limbs as previously described (*5*). For this, mice were sacrificed by asphyxiation under $CO_2$ followed by cervical dislocation. The skin near the hind limbs area was sterilized using 70% alcohol and then shaved using a razor blade. Both TA and two Gastroc muscles were recovered from each mouse, and then rinsed twice in pre-warmed (37°C) 1X PBS and then transferred to 60 mm sterile cell culture dish for mincing to ~1 $mm^3$ pieces using fine scissors. Muscle tissue was digested in Collagenase (Sigma-Aldrich, Cat # C0130-1G) (1 mg/ml) and neutral protease, Dispase II (Roche, Cat # 0492078001) (2.4 U/ml) for up to 90 min. The digested muscle mixture was then carefully triturated and passed consecutively through 100 µm and 40 µm pore size nylon mesh filters. The filtrate was then spun at 350x*g* for 10 min for MuSCs before they were either processed for fluorescent activated cell sorting (FACS).

**FACS purification of MuSCs**

MuSCs were prepared from mice that were sacrificed at 28h post-cardiotoxin injury. MuSCs were prepared from injured TA and Gastroc muscles as described above. The cell pellet obtained from 40 µm strained muscle prep was treated with red blood cell lysis buffer (Sigma-

Aldrich, Cat # R7757-100ML) for 1 min. After lysis, the cell suspension was supplemented with 10 mL of FACS buffer (PBS containing 10% FBS and 3 mM EDTA) and centrifuged for 10 min at 350x*g*. The recovered cell pellet was resuspended in 3 ml of FACS buffer, to which Sytox Green (Life Technologies, Cat # S7020) was added to a final concentration 10 nM for staining the dead cells. Live MuSCs ($TdTomato^+$/Sytox Green) were sorted into microfuge tubes containing FACs buffer. The recovered MuSCs were cultured in Ham's F10 media (Wisent Biocenter) containing 20% bovine growth serum (Thermo Scientific, Cat # SH3054103), supplemented with bFGF (Millipore, Cat # GF003AF-MG) (2.5 ng/ml) and Penicillin-Streptomycin antibiotic (Wisent Biocenter).

**Analysis of MuSC Proliferation and Differentiation**

MuSCs that had not undergone *in vivo* deletion of the floxed alleles, cells were isolated as described in the previous sections (*8*). Mononuclear cells from mouse muscles, that had not undergone *in vivo* deletion of the floxed alleles, were enriched for MuSCs by pre-plating on plastic culture dishes. Starting 40h after isolation, MuSC were incubated in media containing 4-hydroxytamoxifen (2.5 μM final concentration) for 48h to delete the desired allele. Subsequently, cells were cultured in tamoxifen free media for 24h before they were plated for proliferation/differentiation studies. Proliferation studies were performed by allowing MuSCs to grow on collagen coated dishes for 48h. Cells were then mildly trypsinized and detached from plate. Cells were counted using hemocytometer and then plated on collagen-coated 6 well-dishes at a density of 20,000 cells per well. Cells were then counted every 24h for a period of 72h to measure proliferation.

For differentiation studies, MuSCs were allowed to grow on collagen-coated dishes. After 72h of proliferation, cells were mildly trypsinized and seeded at a density of $5x10^5$ cells per well on a 6-well dish. After 12h, the cells were switched to pro-differentiation medium (2% horse serum supplemented in DMEM with 0.1 % insulin (Sigma-Aldrich, Cat # I0516) and 0.1% transferrin (Sigma-Aldrich, T1283-100MG)). Cells were allowed to differentiate for 36h, before they were fixed with 4% PFA for immunostaining.

**Single myofiber isolation and culture**

Myofibers were prepared from flexor digitorum brevis (FDB) muscles of the rear foot of 12-18 weeks old mice as previously described (*16*). The hindlimb skin was sterilized with 70% ethanol and an incision was made carefully in the ankle region to expose the tendons. The FDB was carefully disconnected from the underlying connective tissue and the connecting tendons at the heal region and digits were carefully cut to recover intact muscle. The FDB muscles from both legs were recovered and then were digested for 2h in collagenase (2 mg/ml) prepared in DMEM. After 2h, FDB muscles were carefully transferred to fresh pre-warmed DMEM in FBS coated 10 cm plates. Muscles were carefully triturated with glass pasture pipette with wide bore (cut end with a file or diamond knife and fire polish). The muscle with intact fibers was then moved to a fresh 10 cm plate with DMEM and triturating was continued. After washing the fibers with fresh DMEM, they fibers were transferred to a dish containing DMEM supplemented with 20% FBS, bFGF (2.5 ng/µl) and 1X pen-strep. Myofibers isolated from WT, JMJD3$^{scKO}$, JMJD3$^{scDD}$ and UTX$^{scKO}$ mice were then transferred to 6 cm dishes and cultured for the indicated length of time (0-72h after isolation). At indicated time points, fibers were collected, and fixed with 4% PFA for 15 min before proceeding to immunofluorescence analysis.

**Immunofluorescence and Immunohistochemistry Analysis of Muscles**

FDB myofibers were prepared from WT, JMJD3$^{scKO}$, JMJD3$^{scDD}$ and UTX$^{scKO}$ mice expressing the TdT$^{+}$ lineage specific reporter. MuSCs on the myofibers were visualized based on their TdT$^{+}$ expression. To visualize other proteins, myofibers were quenched and permeabilized with 0.1% Triton-X-100 in PBS containing 100 mM glycine. Subsequently, fibers were blocked for 2h at 22°C then incubated overnight with the indicated antibodies such MyoD1 (1:400, Abcam, Cat#ab133627), JMJD3(1:30) (*32*), UTX (1:40, Santa Cruz). The recovered myofibers were washed three times with 1X TBST and then incubated for 1h with secondary Alexa-Fluor antibodies were added and incubated for 1h. Subsequently, myofibers were washed three times with 1X TBST and counterstained for nuclei with DAPI before mounted on to the glass slides.

Fluorescent labelling of hyaluronic acid was performed using biotinylated hyaluronic acid binding protein (HABP – AMSBIO cat # AMS.HKD-BC41). TA muscles that were harvested at 40h post cardiotoxin injection were in situ fixed with 4% PFA overnight at 4°C. Subsequently the muscles were rehydrated in 15% and 30% sucrose consecutively, before they were frozen in OCT

media. Cryosections (12 μm) were prepared and blocked with 1% bovine serum albumin before they were incubated with biotinylated HABP for 1h at 22°C. Slides were washed and incubated with streptavidin-488 for 1h at 22°C. Slides were then washed and counterstained with DAPI for 5 min before they were quenched with 1X TrueBlack Lipofuscin autofluorescence quencher (Biotium Cat # 23007). After incubation with quencher for 2 min, the slides were washed three times in 1X PBS and were mounted with coverslips to observe under the microscope. All the images were obtained using Zeiss Z1 inverted epiflourescent microscope.

**Preparation of muscle extracts**

Damaged muscle extracts were prepared from WT mice (10-14 weeks old) as previously described (*20*) with minor modifications. TA and Gastroc muscles were damaged with 40 μl and 60μl of cardiotoxin respectively. Mice were maintained for 30h post-injury and then euthanized. The damaged hindlimb muscles were harvested on ice, and the tendons along with epidermal and fatty layers were carefully removed. The weight of the recovered muscle tissue was recorded prior to extraction. The muscle tissue was finely minced with scissors followed by chopping with a surgical blade in a 6 cm dish containing DMEM and protease inhibitor cocktail (1 mL of DMEM per 680 mg of muscle tissue). The mixture was transferred to a Dounce homogenizer chilled on ice. The muscle tissue was disrupted with an A-pestle using 2 strokes to generate a homogenous mixture. The resulting homogenate was transferred to a 1.5 ml microfuge tubes and spun at max speed for 20 min at 4 °C. The supernatant was collected and separated into aliquots for freezing in liquid $N_2$. We use 10 μl of muscle extract to treat MuSC/myofibers per mL of media.

For Control and Mdx muscle extracts, the gastrocnemius muscles were harvested, and the epithelial layers were carefully peeled off before mincing the muscle tissue with scissors in the presence of DMEM and protease inhibitor cocktail. The minced muscle tissue was transferred to Dounce homogenizer, and the tissue was further disrupted in 2 strokes with A-pestle on ice. The homogenate was spun and stored as described in the previous paragraph.

**EdU-based activation assay**

Activation of MuSCs was measured using EdU (5-ethynyl -2'deoxyuridine). EdU (10 mg/ml in 95% Saline + 5 % DMSO) was injected intraperitoneally (*i.p.*) into the mice at 28h post cardiotoxin injury. Mice were sacrificed 12h after EdU injections, and the damaged TA and

Gastroc muscles were harvested from the hind limbs as described above. After removing red blood cells, the heterogenous mixture of cells were fixed in 4% PFA for 15 minutes. Cells were centrifuged at 1800x*g* for 5 min at 4°C and then were then permeabilized by treatment with D-PBS (containing 0.1% Triton-X-100 and 100 mM glycine) for 7 min. Cells were washed twice with 3% BSA and then EdU Click-iT reaction was performed using Click-iT™ EdU Alexa Fluor™ 488 Flow Cytometry Assay Kit (Thermo-Fisher Cat# C-10420). The number of cells having proceeded into S-phase of the cell cycle was measured as a percentage of $TdT^+$ cells that were also $EdU^+$.

For *ex vivo* activation assays, cells were isolated from TA and Gastroc muscles of mice that had (or had not) previously been subjected to an injury on the contralateral leg. EdU (1 μM, final concentration) was added to the cultures of MuSCs at 24h post-isolation. Cells were harvested 12h later and fixed in 4% PFA prior to permeabilization with Triton X-100 in glycine PBS for 5 min. EdU Click-iT reaction was performed and percentage of $EdU^+/TdT^+$ cells was measured by FACS to report *ex vivo* activation potential.

***EdU assay on Myofibers***

Myofibers were prepared as described above. EdU was added to the myofibers 24h post isolation. For rescue experiments involving addition of hyaluronic acid (HA), HA was added at 12h post isolation of the myofibers at a concentration of 2.5 μg/ml of culture media. Damaged muscles extract (final conc 10 μl/mL of 680g tissue /mL extract) was added to myofibers immediately after isolation as a supplement to the myofiber culture media. Similarly, treatment of myofibers with IFNγ (50 ng/ml of culture media) occurred immediately after isolation.

**Preparation of protein extract and immunoblotting**

Cultured MuSCs were harvested, and cells were disrupted in lysis buffer (10 mM Tris, pH6.8; 150 mM NaCl; 1% Triton-X-100 and protease inhibitor cocktail). Cells were incubated for 15 min on ice with intermittent tapping and then centrifuged at maximum speed (14,000x*g*) for 10 min. Supernatants were recovered and their protein content was estimated using Bradford's regent. Equal amounts (20 μg) of protein were loaded on 8% polyacrylamide gels and transferred to nitrocellulose membranes which were immunoblotted with indicated antibodies. Alexa fluor secondary antibodies (Jackson Immuno Research) were used at a dilution of 1 in 5000. The

membranes were washed three times with 0.1% Tween containing 1X TBS, and immunoblotted proteins were detected using a Bio-Rad ChemiDoc MP system.

**Preparation of RNA and RT-qPCR**

Total RNA was extracted using TRIZol (Thermo Fisher Cat # 15596026) as per manufacturer's instructions. RNA was estimated using Thermo Scientific Nanodrop. M-MuLV reverse transcriptase (New England Biolabs, Cat # M0253L) was used to convert 1 µg of RNA to cDNA following the protocol recommended by the manufacturer. Quantitative real time PCR was performed on Rotor-Gene Q Qiagen PCR system. Relative mRNA abundance was measured using GAPDH as internal control and by calculating ΔΔCt. Sequences of primers used in the study are reported in the **Primers Table (**below**).**

**Single-cell RNA-Sequencing**

Mononuclear cells were isolated from injured TA and Gastroc muscles of WT, JMJD3$^{scKO}$, and UTX$^{scKO}$ mice at 40h post injury in triplicate. MuSCs were purified from mononuclear cells by FACS (Sytox Green$^{-}$/TdT$^{+}$) into microfuge tubes with 2% BSA in PBS. FACS enriched MuSCs from WT (1402 cells), JMJD3$^{scKO}$ (1074 cells), and UTX$^{scKO}$ (713 cells) mice were then subjected to droplet-based single cell RNA Sequencing (scRNA-Seq) on the 10X Genomics Chromium platform. Libraries were constructed using the Single Cell 3' Reagent kit v3 and sequenced on the Illumina NovaSeq 6000 platform to obtain ~20,000 reads per cell.

**Bulk RNA-Sequencing**

MuSCs (FACS sorted for TdT expression) were isolated from damaged TA and Gastroc muscles at 30h post-injury as described above. RNA was prepared from MuSCs using NucleoSpin RNA Plus XS kit (Macherey-Nagel, Cat # 740990.50) according to the manufacturer's protocol. Total RNA was rRNA depleted using Kapa stranded depletion rRNA kit and cDNA library was prepared using a KAPA stranded mRNA sequencing kit according to the manufacturer protocol. Sequencing was performed on an Illumina NovaSeq 6000 platform using the 50 nt paired end reads protocol.

**Genome wide binding studies using Cleavage under targets and Tagmentation (CUT&Tag)**

MuSCs (FACS sorted for TdT expression) were isolated from damaged TA and Gastroc muscles at 30h post injury as described above. MuSCs (60,000 cells) were bound to concanavalin A beads and CUT&Tag was performed with indicated antibodies as previously described (*33*). Libraries were sequenced on Illumina NovaSeq 6000 platform. Analysis was performed using our previously described pipeline (*33*).

**Analysis of Single-Cell RNA-Sequencing**

Filtered count matrix from 10X CellRanger v2.1.1 was used for downstream analysis of scRNA-Seq data. Quality control analysis, filtering, and normalization of scRNA-seq data was performed using SCANPY toolkit (*34*) in Python. Cells with less than 200 detected genes per cell were filtered. To remove low quality or dead cells, the fraction of mitochondrial genes transcription was calculated and cells with more than 10% of mitochondrial genes were eliminated from the downstream analysis. Furthermore, genes that appeared in less than three cells were filtered out. To remove immune cells from the analysis, cells with high expression level of Cd14, S100a8, and Ly6a were eliminated. To facilitate comparison of count values between cells, each cell was normalized by total counts over all genes and log transformed.

To explore the main axis of data variation, selected variable genes were used for principal component analysis (PCA) and dimensional reduction of data. By choosing 50 as number of PCs and 20 as number of neighbors, we embedded the data in two dimensional UMAP manifold. To classify cells based on similarity in gene expression signatures, Leiden clustering with resolution = 1 was employed. To annotate each cluster, we plotted mean expression level of a set of genes as dot plot. To perform trajectory analyses, Palantir workflow (*35*) was applied, and the cell densities in each sample were calculated in t-SNE manifold.

**Generating gene signatures for annotating cell types in single-cell RNA-seq**

Gene sets corresponding to signatures for quiescent, proliferating and activated muscle stem cells were derived from differentially expressed genes (DEGs) identified in published RNA-seq data (GEO accession: GSE113631) (*22*). Paired-end FASTQ reads corresponding to each condition (n = 2) i.e. “quiescent” (GSM3110518), “proliferating” (GSM3110523, GSM3110524)) and “activated” (GSM3110521, GSM3110522) were retrieved and transcripts corresponding to

Gencode M25 (mm10) were quantified. By setting each condition as the reference, two lists of DEGs were obtained per condition. For example, when replicates corresponding to proliferating stem cells were set as the reference, DEGs in activated vs proliferating cells as well as DEGs in quiescent vs proliferating cells were obtained. The top 50% of the significantly upregulated genes (i.e., adjusted p value < 0.05 and log2foldchange > 0) were retained. The two gene lists per condition were consolidated by finding the common genes and selecting the top 150 genes as the "signature". A unique score is calculated per cell and signature. For each cell in the single-cell RNA-seq dataset, the genes are ranked based on expression (highest to lowest) and only the top 5% are retained. The signature score for that cell is then calculated as the number of genes in the signature found in this ranked-gene-list as a proportion of the total number of genes in the ranked-gene-list.

**Analysis of Bulk RNA-seq**

Bulk RNA-Sequencing was analyzed as previously described (*5*). The list of DEGs was filtered and significant DEGs identified using the adjusted *p* value cutoff of 0.05. Gene Set Enrichment Analysis (GSEA) (*24*) with the DEGs using various datasets from the Molecular Signature Database v7.2 (i.e. REACTOME, KEGG, GO and Hallmarks) was performed using the R-package fgsea v1.14.0.

**Measuring IFNγ levels in muscle extracts**

The presence of IFNγ in the muscle extracts is detected by using ELISA MAX$^{TM}$ Deluxe set mouse IFNγ kit (Biolegend, Cat. No. 430804, Lot No. B351388). Corning Costar 96-well high bind assay plates (Ref. 9018) were coated with capture antibody and incubated overnight at 4 °C. The plates were washed and blocked with Assay diluent (from kit supplier) before incubation with the extracts prepared from various muscles. After incubating the antibodies with muscle extracts for 2h, the detection antibody was added. The antibody complex was detected using Avidin-HRP/substrate solution, and the absorbance was measured at 450 nm and 570 nm. The absorbance at 450 nm was subtracted from the absorbance at 570 nm and the resulting values were plotted on the standard curve to obtain IFNγ levels in pg/mL.

**Statistics in study**

Statistical analysis was performed using GraphPad Prism (version 8.4.3). For myofiber cross-sectional area, statistical significance was determined using an ANOVA test. For all MuSC experiments examining EdU incorporation as well as RT-qPCR analysis, we applied non-parametric, unpaired comparisons using a Student's *t*-test. The distribution of data points is expressed as mean ± SD. When significant, symbols are represented as follows: * $p<0.05$; ** $p<0.01$; *** $p<0.001$; **** $p<0.0001$. All experiments were performed using at least 3 biological replicates and were repeated a minimum of twice. For GSEA, statistical significance was calculated using the algorithm-based approach which randomly re-organized our JMJD3 RNA-Seq dataset into 1000 different permutations and re-performed the Enrichment score analysis. The *p*-val is an estimate of the difference in enrichment score between the calculated enrichment score and the 1000 different null-enrichment scores.

**Schematic representations**

Schematic illustrations in the manuscript were prepared using BioRender online tools under license for publication.

**Primer Table (oligo sequences)**

| Primer Name | Sequence (5' to 3') |
|---|---|
| ROSA26 Tdt WT Forward | AAGGGAGCTGCAGTGGAGTA |
| ROSA26 Tdt WT Reverse | CCGAAAATCTGTGGGAAGTC |
| ROSA26 Tdt Flox Forward | GGCATTAAAGCAGCGTATCC |
| ROSA26 Tdt Flox Reverse | CTGTTCCTGTACGGCATGG |
| Gaka Cre Fwd Common | GCTGCTGTTGATTACCTGGC |
| Gaka Cre Rev WT | CTGCACTGAGACAGGACCG |
| Gaka Cre Rev MUT | CAAAAGACGGCAATATGGTG |
| UTX gn-2 | AGTTTCAGGATACCTTTACTATAAG |
| UTX-24F | CATCAAGAAAATAACAACTTCTGTTCAGT |
| Jmjd3(37584)F | CAGAGGCAGGTAGATCTTTG |
| Jmjd3(37584)F3 | GAGGTGAAGAACGTCAAGTC |
| Jmjd3(37584)R | CAACCCTCCCTTTCTTTTCG |
| JMJD3 KI-F | GCTATACATGAAGGTCCCTGGC |
| JMJD3 KI-WR | GAGCAGAAATTGTTATTCTCTTGGTG |
| JMJD3 KI-MR | AGCAGAAATTGTTATTGGCTTGAGC |
| Ccl2_cDNA_FP1 | AGGTCCCTGTCATGCTTCTG |
| Ccl2_cDNA_RP1 | TCTGGACCCATTCCTTCTTG |
| Tap1_cDNA_FP1 | CGTGTGCACAGAGAGGTGTT |
| Tap1_cDNA_RP1 | AGGTTGATCAGGGTGACCAG |

**Antibodies Used**

| **Antibody** | **Company, Catalogue Number** |
|---|---|
| Anti - JMJD3 | Not commercial (*32*) |
| Anti - UTX | Santa Cruz, SC514859 |
| Mouse monoclonal anti-Pax7 | Developmental studies Hybridoma Bank, Cat No. AB2299243 |
| Anti - MyoD1 | Abcam, Cat No. ab133627 |
| Anti - Tubulin | Sigma, T6557 |
| Anti - H3K27me3 | Cell Signaling, C36B11 |
| Anti - H3K4me3 | Millipore, 07-473 |
| Anti - Pan-Histone H3 | Thermo-Fisher, 701517 |

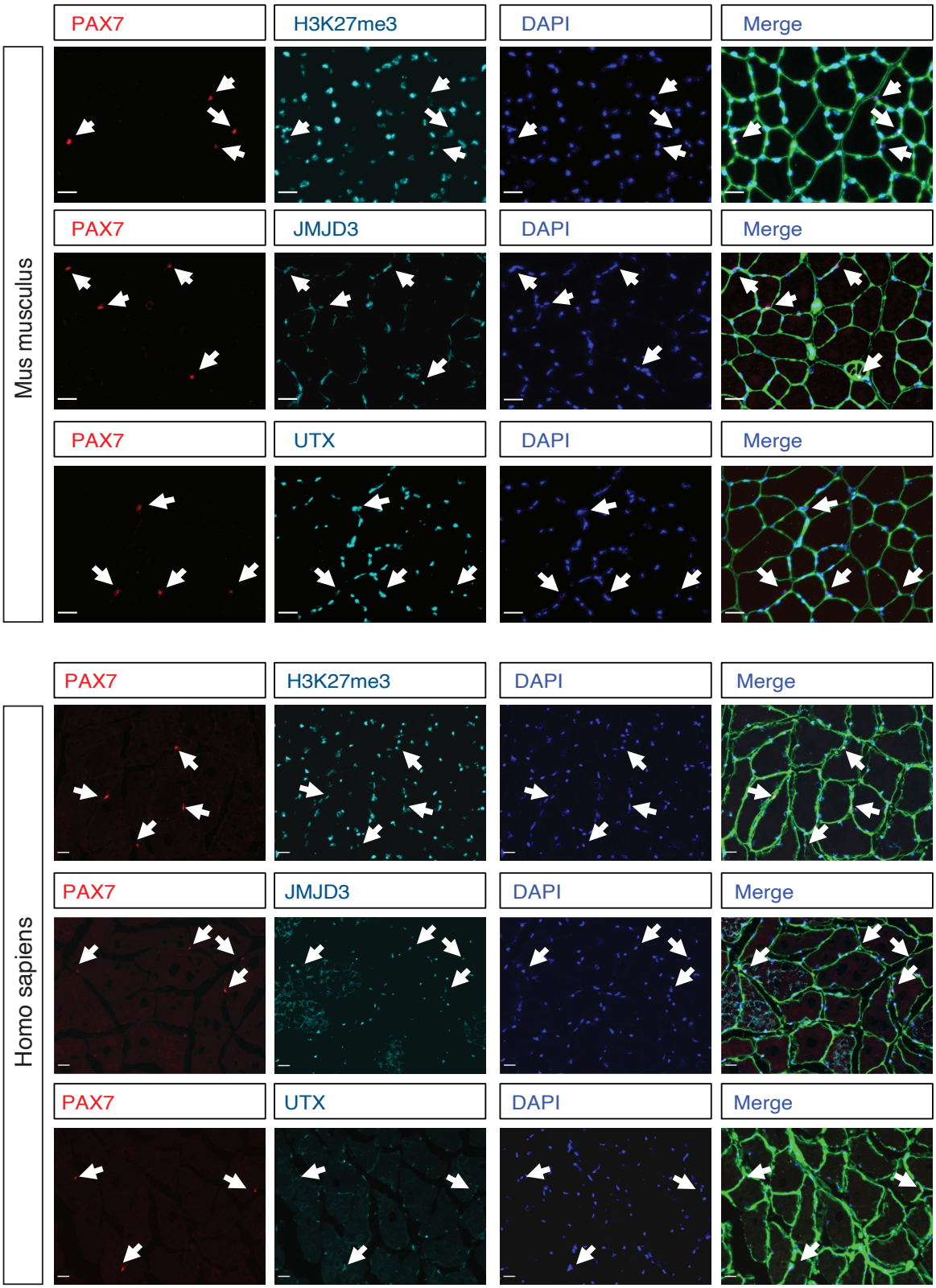
Mus musculus
PAX7
H3K27me3
DAPI
Merge
PAX7
JMJD3
DAPI
Merge
PAX7
UTX
DAPI
Merge
Homo sapiens
PAX7
H3K27me3
DAPI
Merge
PAX7
JMJD3
DAPI
Merge
PAX7
UTX
DAPI
Merge

**Fig. S1. KDM6 family members JMJD3 and UTX are ubiquitously expressed in healthy muscle, including quiescent MuSCs.** Cross-sections from healthy mouse (tibialis anterior) or human (semitendinosus) muscles were analyzed by immunofluorescence using antibodies recognizing Pax7, JMJD3, UTX and H3K27me3. All cells including $Pax7^+$ MuSCs, showed expression of JMJD3, UTX and H3K27me3. Scale bar represents 25 μm.

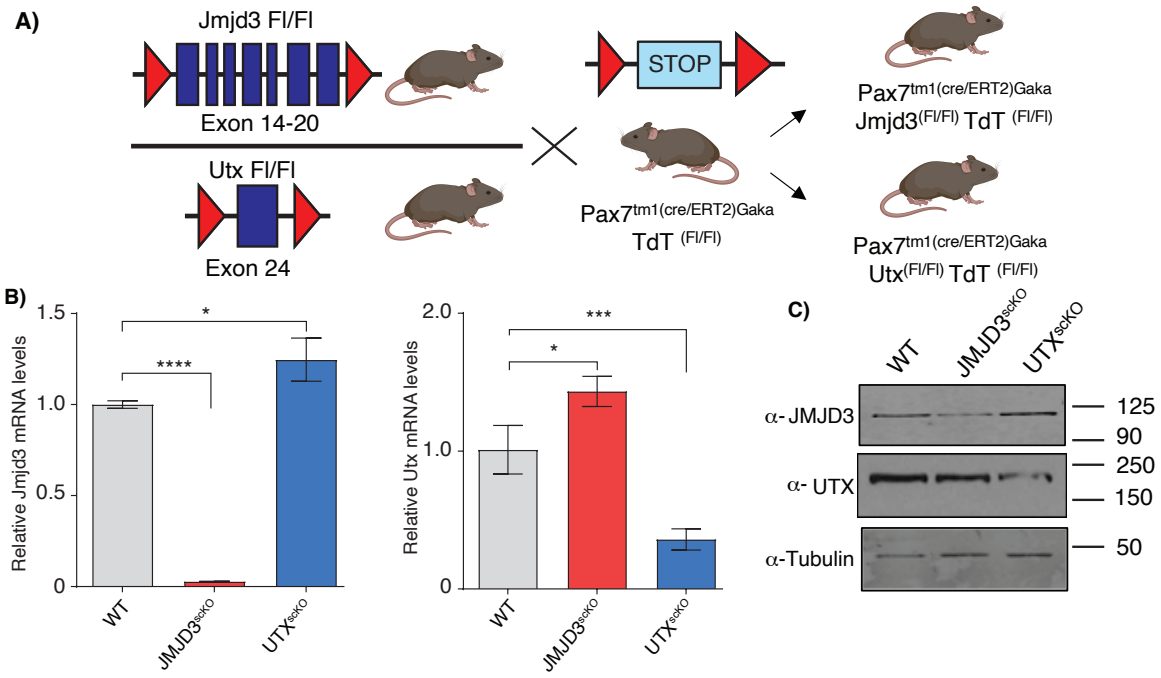


**Fig. S2. Characterization of JMJD3 and UTX MuSC-specific conditional knockout mice. A)** A schematic representation showing *Jmjd3*-floxed Kdm6b$^{tm1Mag}$ mouse floxed at exons 14 - 20 and *Utx*-floxed Kdm6a$^{tm1.1Kaig}$/J mouse floxed at exon 24, crossed with *Rosa26-loxp-STOP-loxp-TdTomato* harboring Pax7$^{tm1(cre/ERT2)\ Gaka}$ mouse to generate JMJD$^{scKO}$ (Pax7$^{CreER}$/JMJD3$^{fl/fl}$/TdT) and UTX$^{scKO}$ (Pax7$^{CreER}$/UTX$^{fl/fl}$/TdT) mice. **B)** Quantification of Jmjd3 and Utx mRNA levels by RT-qPCR in MuSCs isolated from JMJD$^{scKO}$ and UTX$^{scKO}$, validate an efficient deletion of the alleles that results in reduced expression of the genes. Statistical significance was determined using an unpaired *t*-test, * $p<0.05$, *** $p<0.001$, **** $p<0.0001$, n=3. **C)** Western blotting analysis of whole cell protein extracts prepared from JMJD$^{scKO}$ and UTX$^{scKO}$ MuSCs upon Cre-mediated deletion demonstrates loss of JMJD3 and UTX protein expression. Tubulin is used as loading control.

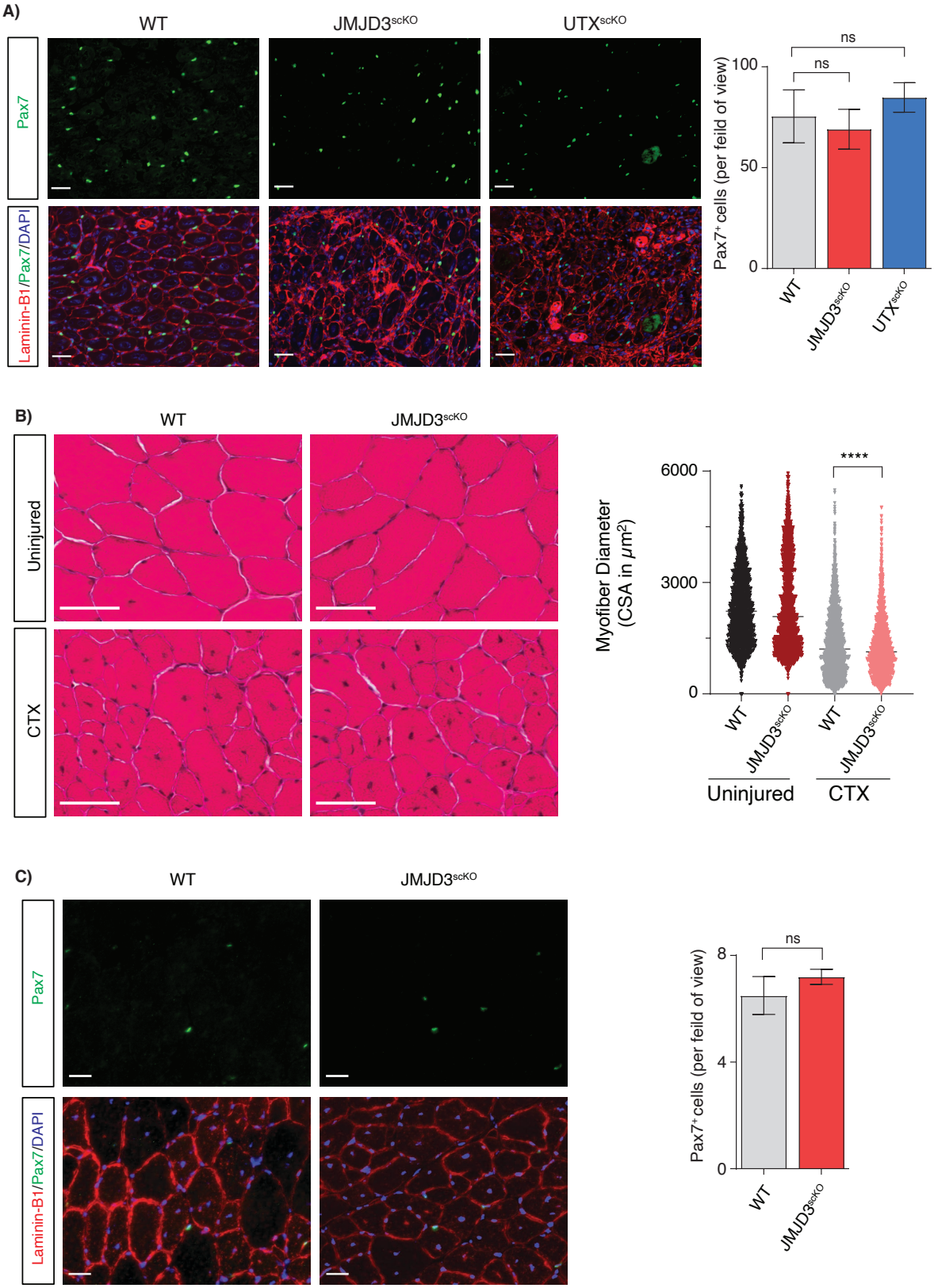
A)
WT
JMJD3scKO
UTXscKO
Pax7
Laminin-B1/Pax7/DAPI
ns
ns
100
50
0
Pax7+ cells (per feild of view)
WT
JMJD3scKO
UTXscKO
B)
WT
JMJD3scKO
Uninjured
CTX
****
6000
3000
0
Myofiber Diameter
(CSA in μm2)
WT
JMJD3scKO
WT
JMJD3scKO
Uninjured
CTX
C)
WT
JMJD3scKO
Pax7
Laminin-B1/Pax7/DAPI
ns
8
4
0
Pax7+ cells (per feild of view)
WT
JMJD3scKO

**Fig. S3. Loss of JMJD3 impairs myofiber regeneration without affecting Pax7$^{+}$ MuSCs – mediated niche repopulation. A)** At 7d post injury, immunofluorescence analysis of TA muscle cross-sections using Pax7 antibody was used to identify and quantitate MuSCs in the regenerating muscle tissue of JMJD3$^{scKO}$, UTX$^{scKO}$, or WT mice. No significant difference in the number of Pax7$^{+}$ MuSCs was observed. Scale bar represents 25 μm. Statistical significance was determined using an unpaired *t*-test, ns = not significant, n=3. **B)** At 21d post-injury, Haematoxylin and Eosin (H&E) staining of TA muscle cross-sections were performed on JMJD3$^{scKO}$ or WT mice. As regeneration progressed to 21d, the myofibers from JMJD3$^{scKO}$ mice continued to show a significant decrease in their cross-sectional area. Scale bar represents 50 μm. Statistical significance was determined using unpaired students *t*-test where **** $p < 0.0001$, n=3 **C)** At 21d post-injury, immunofluorescence analysis was used to measure Pax7$^{+}$ MuSCs cells present in the regenerating muscle. No significant difference in the number of Pax7$^{+}$ cells was observed between WT and JMJD3scKO mice, showing that niche repopulation was not affected by the loss of JMJD3. Scale bar represents 25 μm. Statistical significance was determined using an unpaired *t*-test, ns = not significant, n=3.

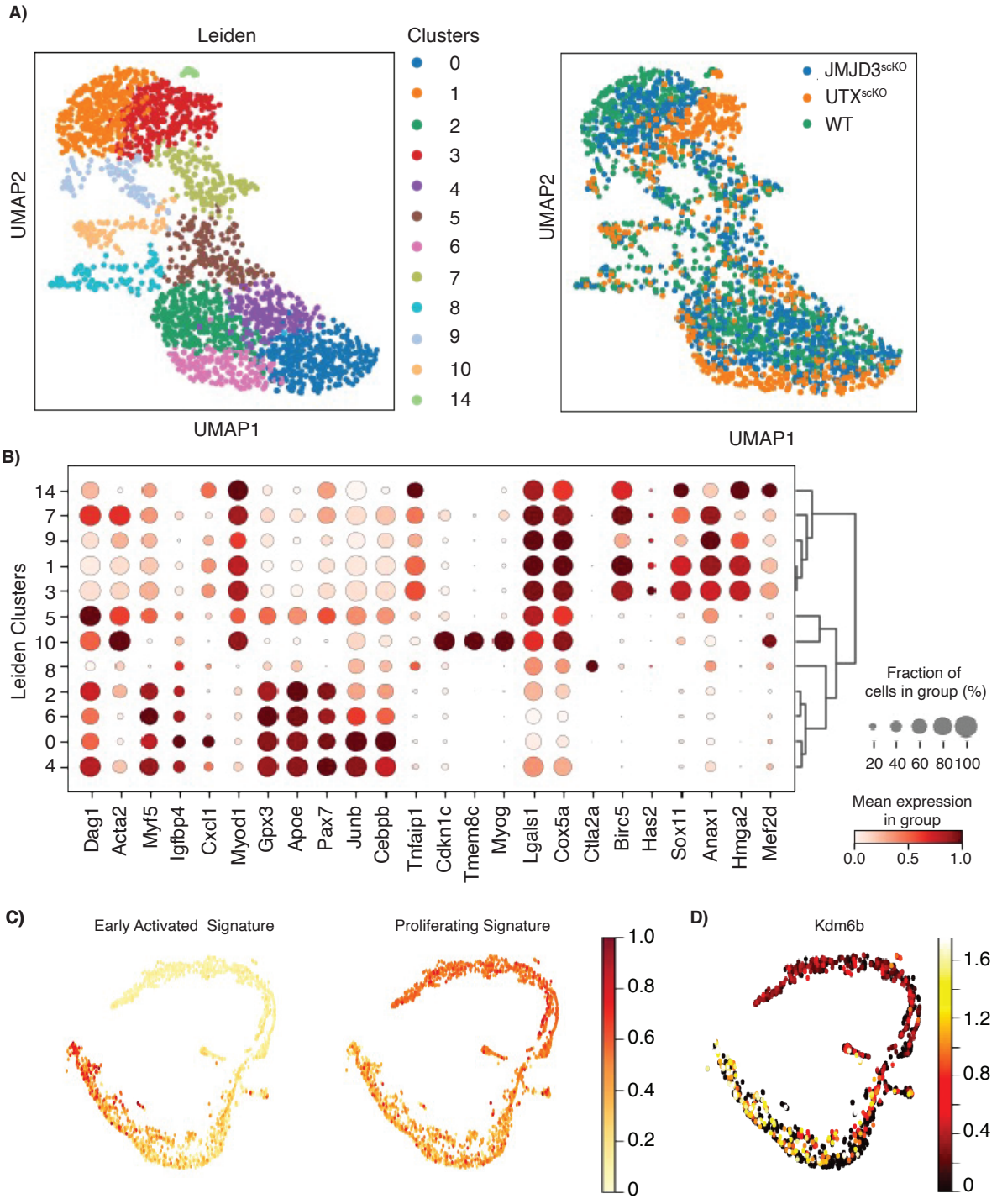
A)
Leiden
Clusters
0
1
2
3
4
5
6
7
8
9
10
14
UMAP2
UMAP1
JMJD3scKO
UTXscKO
WT
B)
Leiden Clusters
14
7
9
1
3
5
10
8
2
6
0
4
Dag1
Acta2
Myf5
Igfbp4
Cxcl1
Myod1
Gpx3
Apoe
Pax7
Junb
Cebpb
Tnfaip1
Cdkn1c
Tmem8c
Myog
Lgals1
Cox5a
Ctla2a
Birc5
Has2
Sox11
Anax1
Hmga2
Mef2d
Fraction of cells in group (%)
20 40 60 80100
Mean expression in group
0.0 0.5 1.0
C)
Early Activated Signature
Proliferating Signature
1.0
0.8
0.6
0.4
0.2
0
D)
Kdm6b
1.6
1.2
0.8
0.4
0

**Fig. S4. MuSCs from JMJD3$^{scKO}$ mice are impaired in their ability to re-enter cell cycle as a response to muscle injury. A)** Single cell RNA-Seq was performed on purified TdT$^{+}$ MuSCs isolated from JMJD3$^{scKO}$ (1074 cells), UTX$^{scKO}$ (713 cells), and WT (1402 cells) mice at a time point of 40h after CTX-muscle injury. UMAP was used to represent the relationship of Leiden clustered cells through dimensional reduction. Datasets for each genotype represent cells isolated from 3 distinct mice. **B)** Dot plot analysis shows the expression of genes that most contributed to the defining of the Leiden clusters in TdT$^{+}$-MuSCs isolated from regenerating muscle at 40h post injury. **C)** Distribution of purified MuSCs across the trajectory and showing enrichment for either early MuSC activation or proliferation MuSC gene signatures. **D)** Expression of Kdm6b/Jmjd3 in individual cells along the trajectory, indicating an increased transcript abundance at early activation of MuSCs.

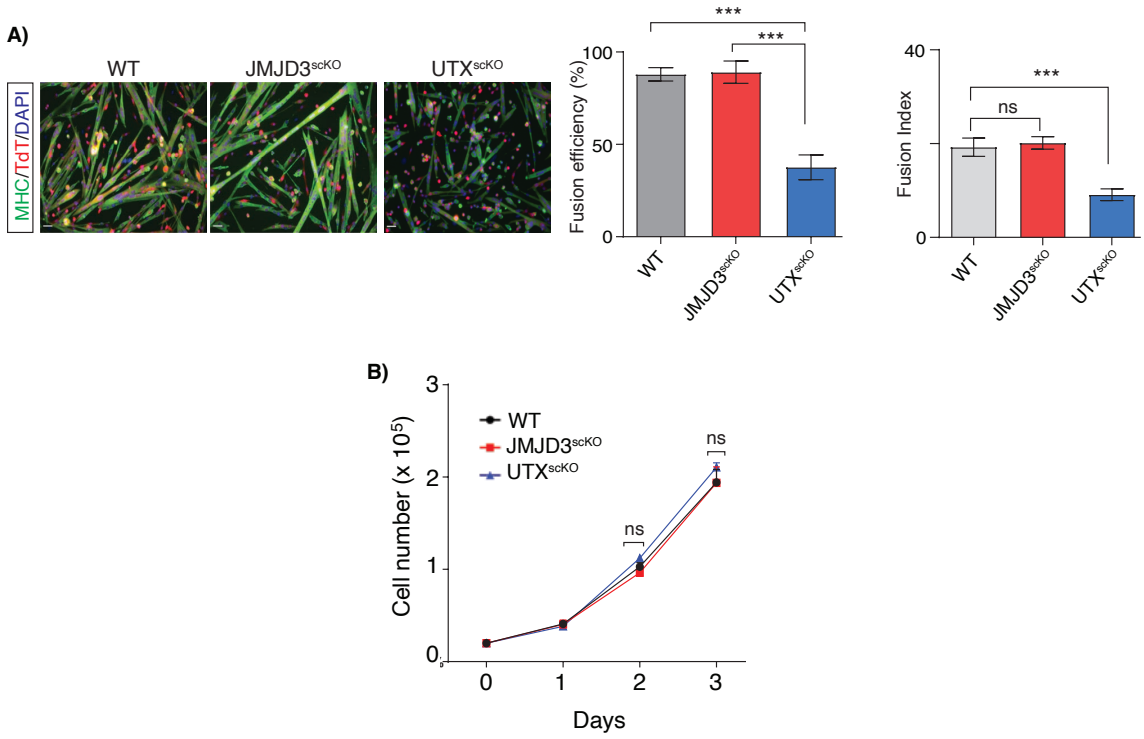


**Fig. S5. UTX is required for terminal muscle differentiation and cannot be compensated by JMJD3. A)** Immunofluorescence analysis of differentiated primary myoblasts prepared from WT, JMJD$^{scKO}$ and UTX$^{scKO}$ mice after Cre-mediated deletion of the floxed alleles. Fusion efficiency was calculated as the percentage of nuclei present in multinucleated myotubes, while Fusion index was calculated by determining the mean number of nuclei per MHC positive myofiber. Scale bar represents 25 µm. Statistical significance was determined using an unpaired *t*-test, ns = not significant, *** $p<0.001$, n=3. **B)** Growth curve of MuSCs isolated from WT, JMJD$^{scKO}$ and UTX$^{scKO}$ mice upon Cre-mediated deletion of JMJD3 and UTX, indicating no significant change in the rate of proliferation.

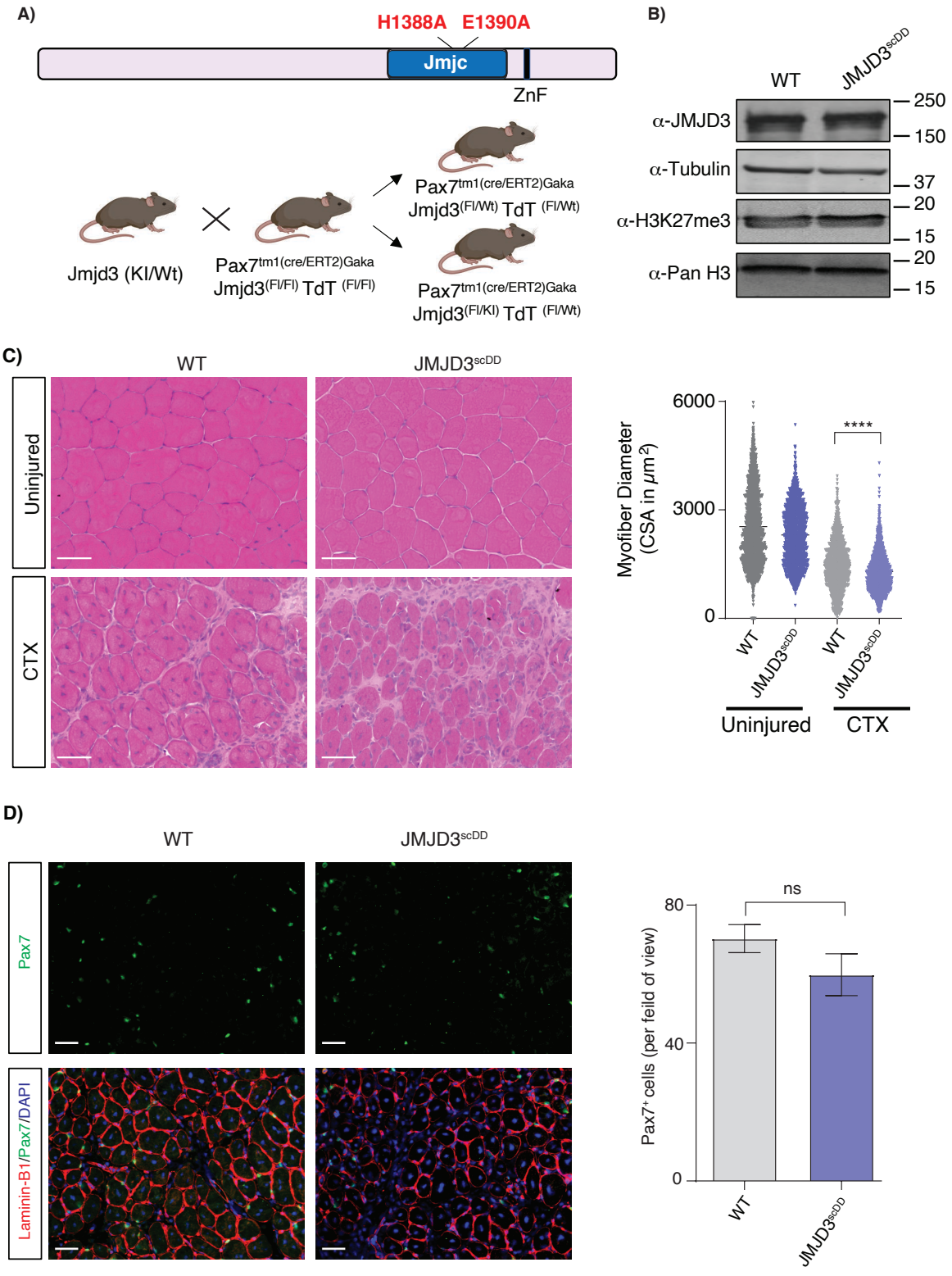
A)
H1388A E1390A
Jmjc
ZnF
Jmjd3 (KI/Wt)
Pax7tm1(cre/ERT2)Gaka Jmjd3(Fl/Fl) TdT (Fl/Fl)
Pax7tm1(cre/ERT2)Gaka Jmjd3(Fl/Wt) TdT (Fl/Wt)
Pax7tm1(cre/ERT2)Gaka Jmjd3(Fl/Kl) TdT (Fl/Wt)
B)
WT
JMJD3scDD
α-JMJD3
α-Tubulin
α-H3K27me3
α-Pan H3
250
150
37
20
15
20
15
C)
WT
JMJD3scDD
Uninjured
CTX
Myofiber Diameter (CSA in μm2)
6000
3000
0
****
WT
JMJD3scDD
WT
JMJD3scDD
Uninjured
CTX
D)
WT
JMJD3scDD
Pax7
Laminin-B1/Pax7/DAPI
Pax7+ cells (per feild of view)
80
40
0
ns
WT
JMJD3scDD

**Fig. S6. H3K27-demethylase activity of JMJD3 is required for MuSC activation after injury.** Mice lacking H3K27-demthylase activity of JMJD3 (JMJD3$^{scDD}$) were generated by CRISPR/Cas9 mediated recombination to introduce point mutations (H1388A and E1390A) in the Jmjc domain of the protein. **A)** Schematic representation highlighting the position of mutant residues within the Jmjc domain that produced demethylase dead JMJD3 (JMJD3$^{scDD}$) mice by crossing with Pax7$^{CreER}$/JMJD3$^{fl/fl}$/TdT mice. **B)** Western Blotting analysis of whole cell protein extracts prepared from JMJD$^{scKO}$ and JMJD3$^{scDD}$ MuSCs upon Cre-mediated deletion demonstrates expression of JMJD3 protein, while increase in H3K27me3 levels in JMJD3$^{scDD}$ protein extracts. Pan-H3 and tubulin were used as loading controls. **C)** Haematoxylin and eosin staining of JMJD3$^{scDD}$ TA muscle cross-sections at 7d post CTX-mediated injury. Graph representing the cross-sectional area of regenerated myofibers, indicate a decrease in the myofiber diameter at the end of 7d of regeneration. Scale bar represents 50 μm, n = 3. **D)** Immunofluorescence analysis of TA muscle cross-sections for the presence of Pax7$^{+}$ MuSCs at 7d post CTX-mediated muscle injury in WT and JMJD3$^{scDD}$. No significant difference in the number of Pax7 cells is observed at the end of 7d post muscle injury. Scale bar represents 25 μm, n = 3.

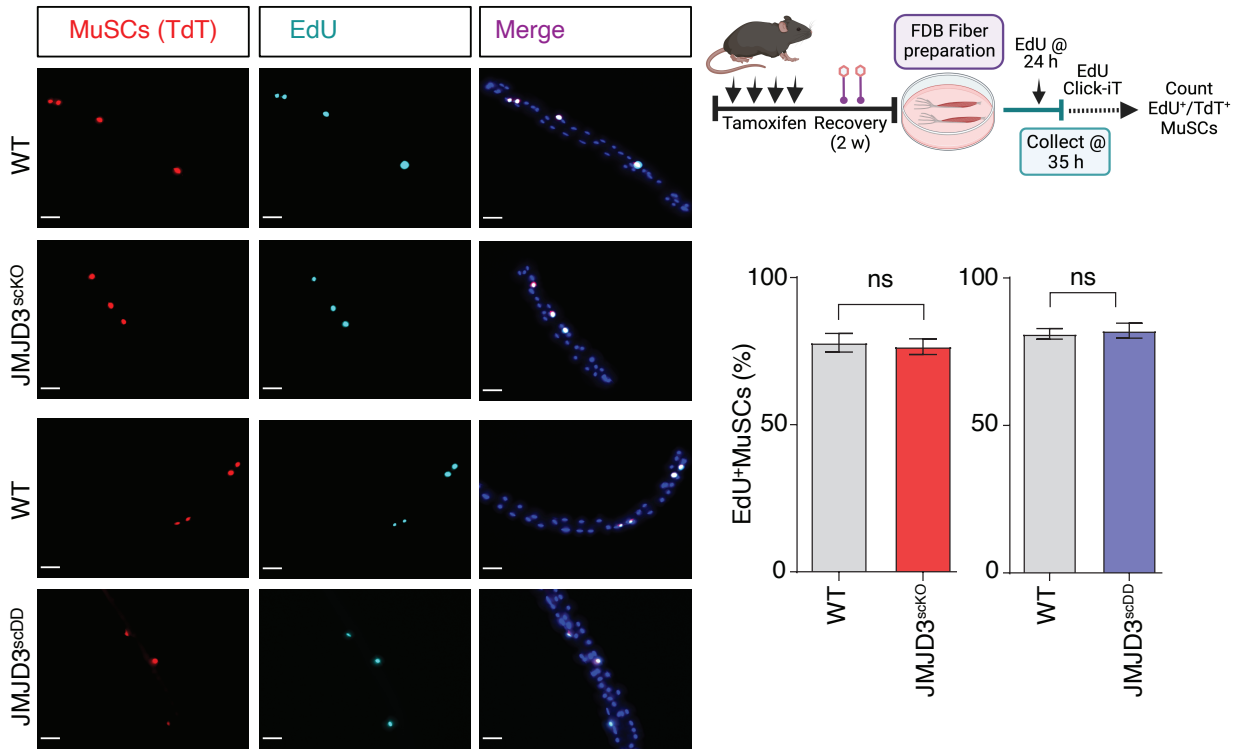


**Fig. S7. JMJD3 is dispensable for activation of MuSCs in the absence of injury.** Myofibers were isolated from Flexor Digitorum Brevis (FDB) muscle of WT, JMJD3$^{scKO}$ and JMJD3$^{scDD}$ mice that were not subjected to any injury. MuSC activation was quantified by measuring *ex vivo* EdU incorporation rate by immunofluorescence analysis (a ratio of TdT+ (Red) and EdU+(Cyan)). In the absence of any muscle injury to the mice, no significant change in the activation of MuSCs was observed. Scale bar represents 25 µm. Statistical significance was determined using an unpaired *t*-test, ns = not significant, n = > 50 fibers for each sample obtained from 2 mice.

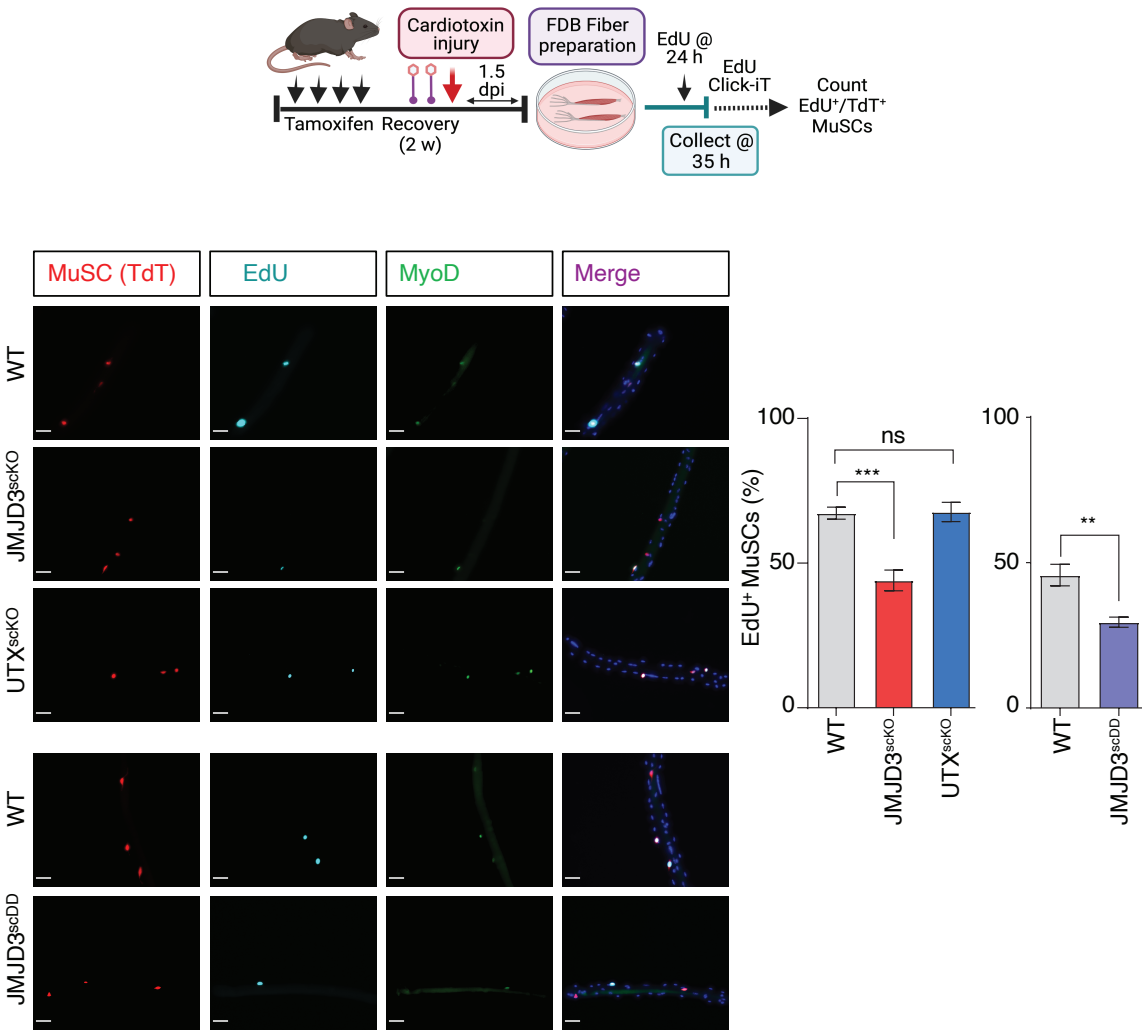


**Fig. S8. Loss of JMJD3 (or its enzymatic activity) impairs activation of MuSCs.** Myofibers were prepared from the FDB muscle of mice that had previously (36h before isolation) received a CTX injury to the TA muscle on the contralateral leg. *ex vivo* activation of MuSCs that was measured as percentage of MuSCs (TdT+) that were positive for EdU (Cyan), showed a significant decrease in the activation of MuSCs on myofibers prepared from JMJD3$^{scKO}$ and JMJD3$^{scDD}$. A schematic outline of this experiment was represented on top right side of the figure. Scale bar represents 25 µm. Statistical significance was determined using an unpaired *t*-test, ns = not significant, ** $p<0.01$, *** $p<0.001$, n = > 50 fibers for each sample obtained from 3 mice.

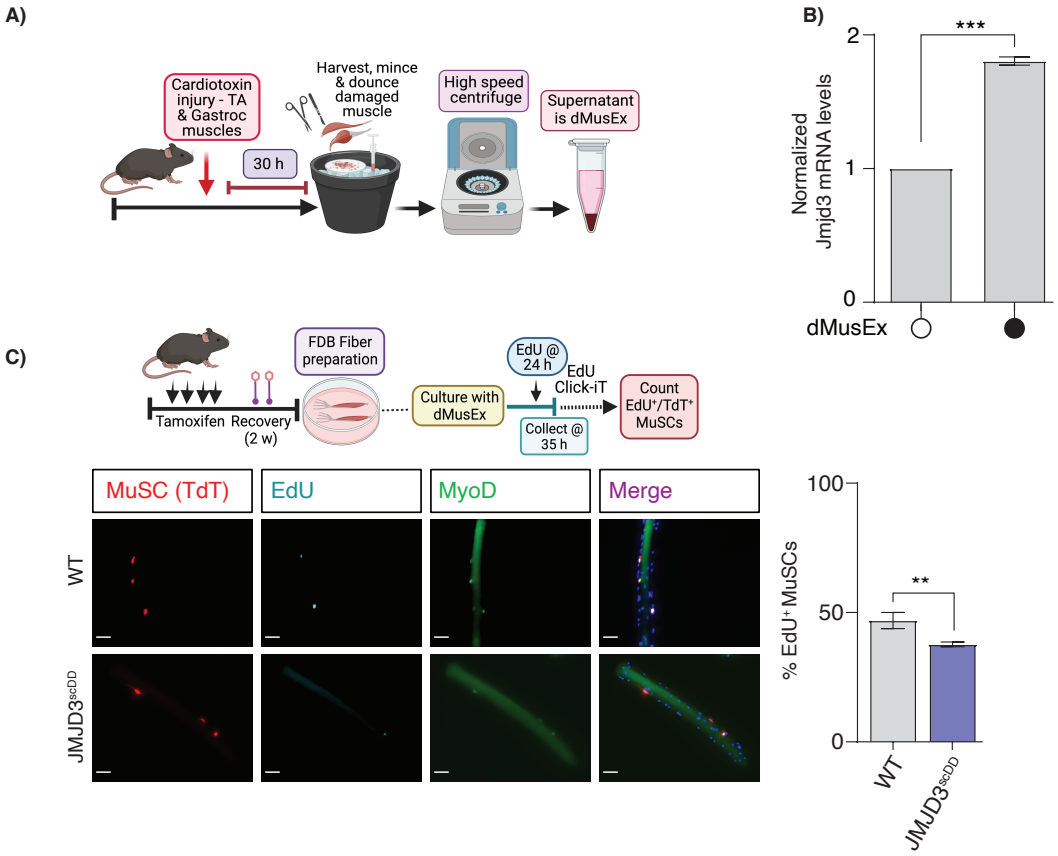


**Fig. S9. Soluble extract from injured muscle blocks activation of JMJD3-null MuSCs. A)** Schematic representation of strategy adapted to prepare damaged muscle extract (dMusEx) prepared from cardiotoxin damaged (30h post-injury) tibialis anterior and gastrocnemius muscles. **B)** RT-qPCR analysis to measure transcript abundance of JMJD3 in MuSCs treated with or without damaged muscle extract. Treatment of MuSCs with damaged muscle extract immediately after isolation showed an increase in Jmjd3 mRNA levels at 30h. **C)** Myofibers were prepared from FDB muscles of JMJD3$^{scDD}$ mice and were cultured in media with damaged muscle extract. *ex vivo* activation of these MuSCs was measured as percentage of MuSCs (TdT+) that were positive for EdU (Cyan). Treatment of MuSCs with damaged muscle extract significantly delayed the activation of MuSCs. Scale bars represent 25 µm. Statistical significance was determined using an unpaired *t*-test, ** $p<0.01$, *** $p<0.001$. n = > 50 fibers for each sample obtained from 3 mice.

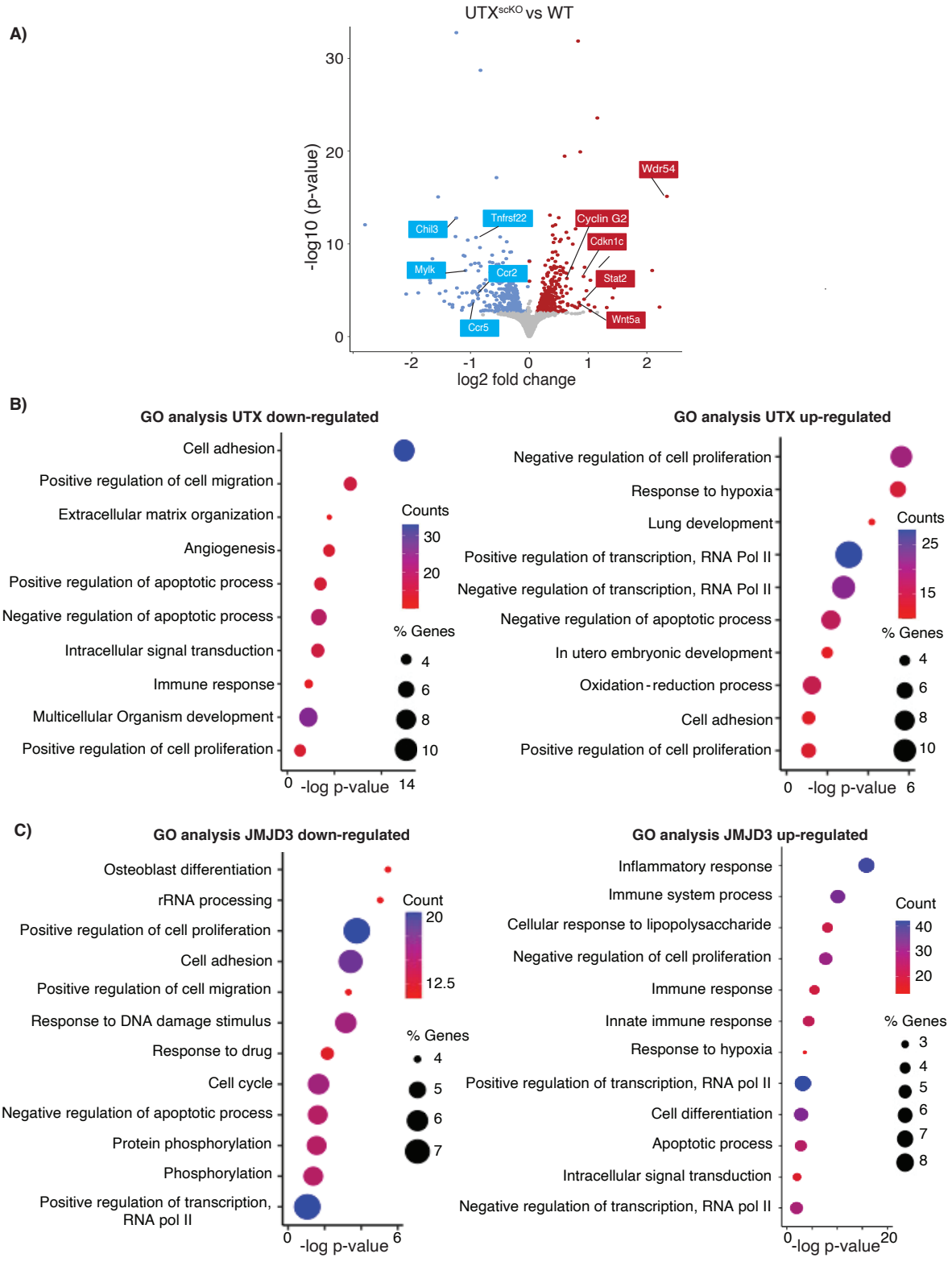
A)
UTX scKO vs WT
-log10 (p-value)
log2 fold change
Wdr54
Chil3
Tnfrsf22
Cyclin G2
Cdkn1c
Mylk
Ccr2
Stat2
Wnt5a
Ccr5
B)
GO analysis UTX down-regulated
Cell adhesion
Positive regulation of cell migration
Extracellular matrix organization
Angiogenesis
Positive regulation of apoptotic process
Negative regulation of apoptotic process
Intracellular signal transduction
Immune response
Multicellular Organism development
Positive regulation of cell proliferation
Counts
% Genes
-log p-value
GO analysis UTX up-regulated
Negative regulation of cell proliferation
Response to hypoxia
Lung development
Positive regulation of transcription, RNA Pol II
Negative regulation of transcription, RNA Pol II
Negative regulation of apoptotic process
In utero embryonic development
Oxidation-reduction process
Cell adhesion
Positive regulation of cell proliferation
Counts
% Genes
-log p-value
C)
GO analysis JMJD3 down-regulated
Osteoblast differentiation
rRNA processing
Positive regulation of cell proliferation
Cell adhesion
Positive regulation of cell migration
Response to DNA damage stimulus
Response to drug
Cell cycle
Negative regulation of apoptotic process
Protein phosphorylation
Phosphorylation
Positive regulation of transcription, RNA pol II
Count
% Genes
-log p-value
GO analysis JMJD3 up-regulated
Inflammatory response
Immune system process
Cellular response to lipopolysaccharide
Negative regulation of cell proliferation
Immune response
Innate immune response
Response to hypoxia
Positive regulation of transcription, RNA pol II
Cell differentiation
Apoptotic process
Intracellular signal transduction
Negative regulation of transcription, RNA pol II
Count
% Genes
-log p-value

**Fig. S10. JMJD3 and UTX regulate distinct cellular process during MuSC activation.** Bulk RNA-Sequencing was performed on $TdT^{+}$ MuSCs purified from WT, $JMJD3^{scKO}$, or $UTX^{scKO}$ mice. **A)** Volcano plot shows the relative transcript levels for genes in activating MuSCs isolated from $UTX^{scKO}$ versus WT mice. **B)** Gene Ontology (GO) analysis was performed on transcripts that showed significant changes in gene expression upon loss of UTX. **C)** Gene Ontology (GO) analysis was performed on transcripts that showed significant changes in gene expression upon loss of JMJD3. These finding show that loss of UTX modifies the expression of genes involved in development and cell adhesion while loss of JMJD3 modifies the expression of genes involved in cell migration and proliferation.

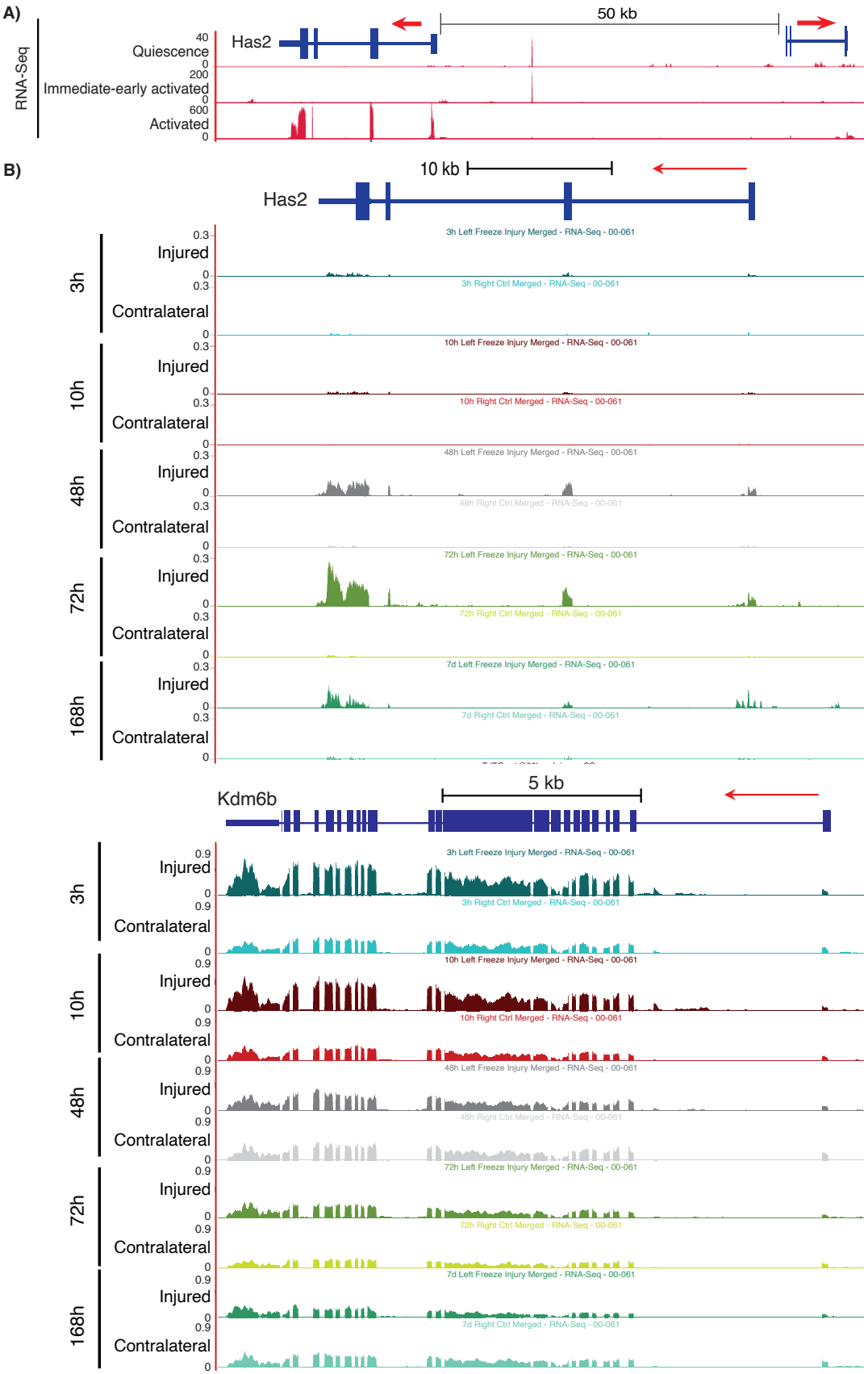
A)
RNA-Seq
Has2
50 kb
Quiescence
Immediate-early activated
Activated
B)
Has2
10 kb
3h
10h
48h
72h
168h
Injured
Contralateral
3h Left Freeze Injury Merged - RNA-Seq - 00-061
3h Right Ctrl Merged - RNA-Seq - 00-061
10h Left Freeze Injury Merged - RNA-Seq - 00-061
10h Right Ctrl Merged - RNA-Seq - 00-061
48h Left Freeze Injury Merged - RNA-Seq - 00-061
48h Right Ctrl Merged - RNA-Seq - 00-061
72h Left Freeze Injury Merged - RNA-Seq - 00-061
72h Right Ctrl Merged - RNA-Seq - 00-061
7d Left Freeze Injury Merged - RNA-Seq - 00-061
7d Right Ctrl Merged - RNA-Seq - 00-061
Kdm6b
5 kb

**Fig. S11. Expression of the Has2 gene is upregulated in MuSC with and without injury. A)** Re-analysis of published RNA-Sequencing experiments *(22)* show that Has2 is not expressed in quiescent MuSCs but is up-regulated as the freshly isolated MuSC progress towards the proliferative state. UCSC browser tracks are shown to indicate the expression landscape of the *Has2* locus in MuSCs that are in either quiescent, immediate-early activated or activated states. **B)** Re-analysis of published RNA-Sequencing experiments *(21)* show that Has2 is up-regulated in regenerating muscle in response to a freeze injury. UCSC browser tracks are shown for the *Has2* and *Jmjd3* genes at various time points after freeze injured while the contralateral muscle serves as an uninjured control. Note that *Kdm6b/Jmjd3* levels are elevated by 3h in response to injury in activation and are restored to basal levels by 48h post-injury.

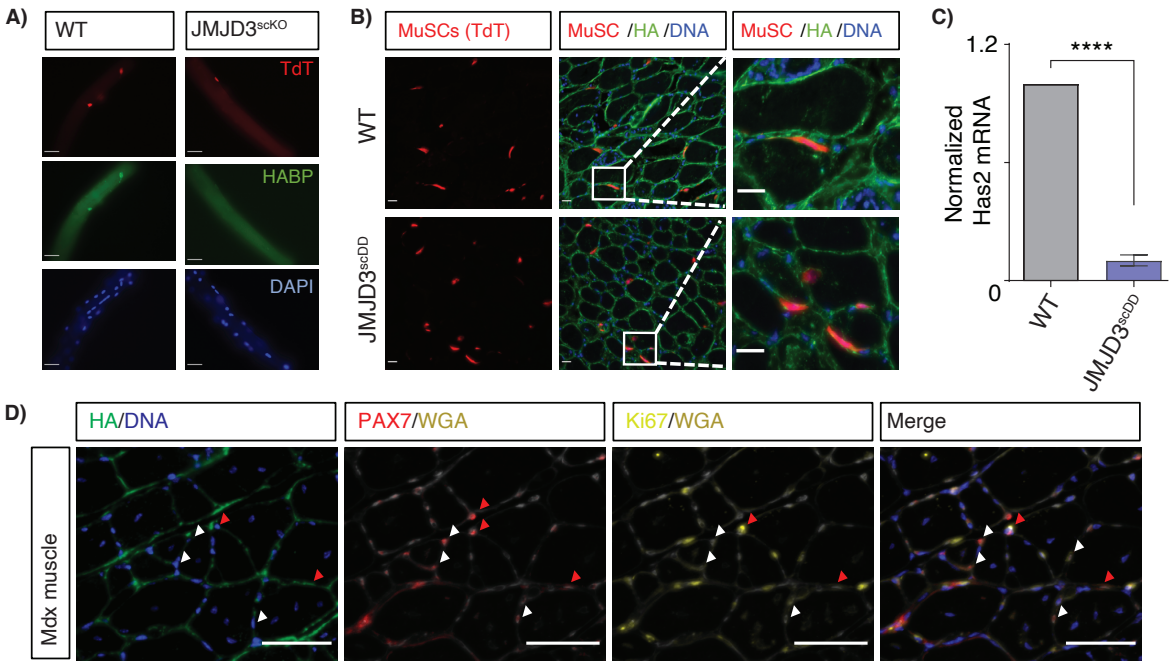


**Fig. S12. Hyaluronic acid incorporation in MuSCs. A)** Immunofluorescence analysis of FDB myofibers for HA incorporation shows the presence of HA in WT MuSCs at 24h after isolation. **B)** Immunofluorescence analysis of TA muscle cross-sections for HABP at 40h post CTX injury from WT, and JMJD3$^{scDD}$ mice. TdT$^{+}$ cells represent MuSCs, HABP represents HA, and DNA is DAPI staining. JMJD3$^{scDD}$ MuSCs show a decrease in the synthesis of hyaluronic acid on the surrounding extracellular matrix. Scale bar represents 25 µm, n = 3. **C)** RT-qPCR analysis of *Has2* mRNA levels in JMJD3$^{scDD}$ MuSCs at 30h post injury show a significant reduction in Has2 mRNA levels. Statistical significance was determined using an unpaired *t*-test, *** $p<0.001$, n = 3. **D)** Activated MuSCs in dystrophic muscle have HA in their extracellular matrix. Immunofluorescence analysis of consecutive TA muscle cross-sectional slices (7 µm) from mdx mice was used to determine the co-localization of activated (Ki-67$^{+}$) MuSCs (Pax7$^{+}$) with hyaluronic acid in their ECM (HABP$^{+}$). Red arrows indicate activated MuSCs (Ki-67+/Pax7+) marked with HABP while white arrows indicate quiescent MuSCs (Ki-67-/Pax7+) that also lack HABP staining.

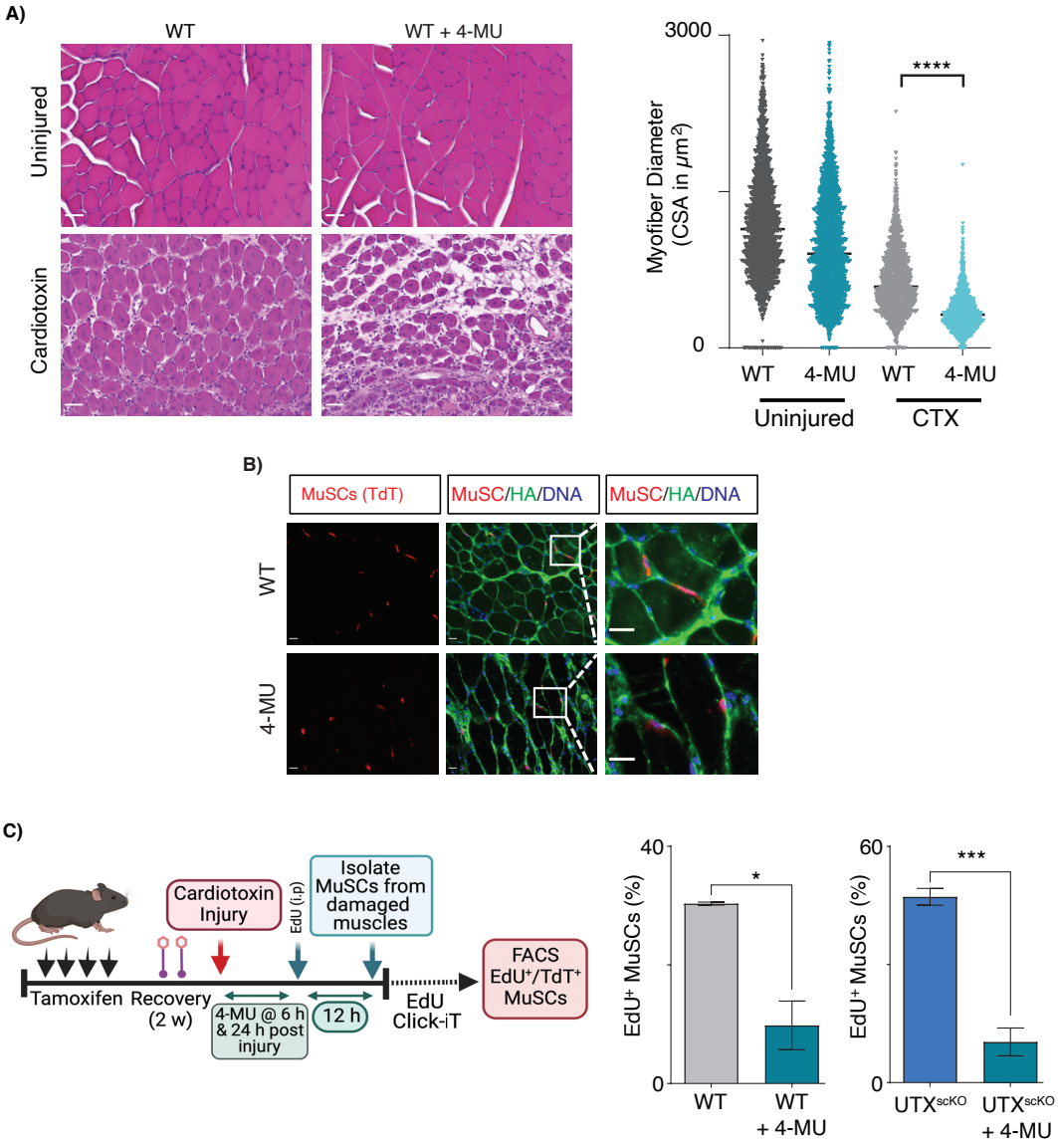


**Fig. S13. Inhibition of HA synthesis impairs regeneration by blocking MuSC activation. A)** Hematoxylin & Eosin staining of TA muscle cross-sections from WT mice that were treated with Has2 inhibitor 4-MU, at 7d post-injury (CTX). Analysis of the histological sections showed fewer myofibers being regenerated and a significant decrease in the cross-sectional area for centrally located regenerating myofibers. Scale bar represents 25 µm, n=3. **B)** Immunofluorescence analysis of TA muscle cross-sections obtained at 40h post CTX injury, from WT mice that were treated with either 4-MU inhibitor or vehicle control. The TdT+ cells represent MuSCs, HABP represents HA, and DNA is DAPI staining. MuSCs in the WT mice treated with 4-MU inhibitor (200 mg/kg) showed a strong decrease in the synthesis of hyaluronic acid in the surrounding extracellular

matrix. **C)** *in vivo* activation of MuSCs in WT mice that were either mock treated or treated with 4-MU at 6 & 24h post-injury. *in vivo* EdU incorporation was used to measure the first passage of cells through S-phase of the cell cycle between 24 and 40h post injury. FACS analysis measured percentage of MuSCs (TdT+) that were positive for EdU. Statistical significance was determined by unpaired *t*-test, n=3.

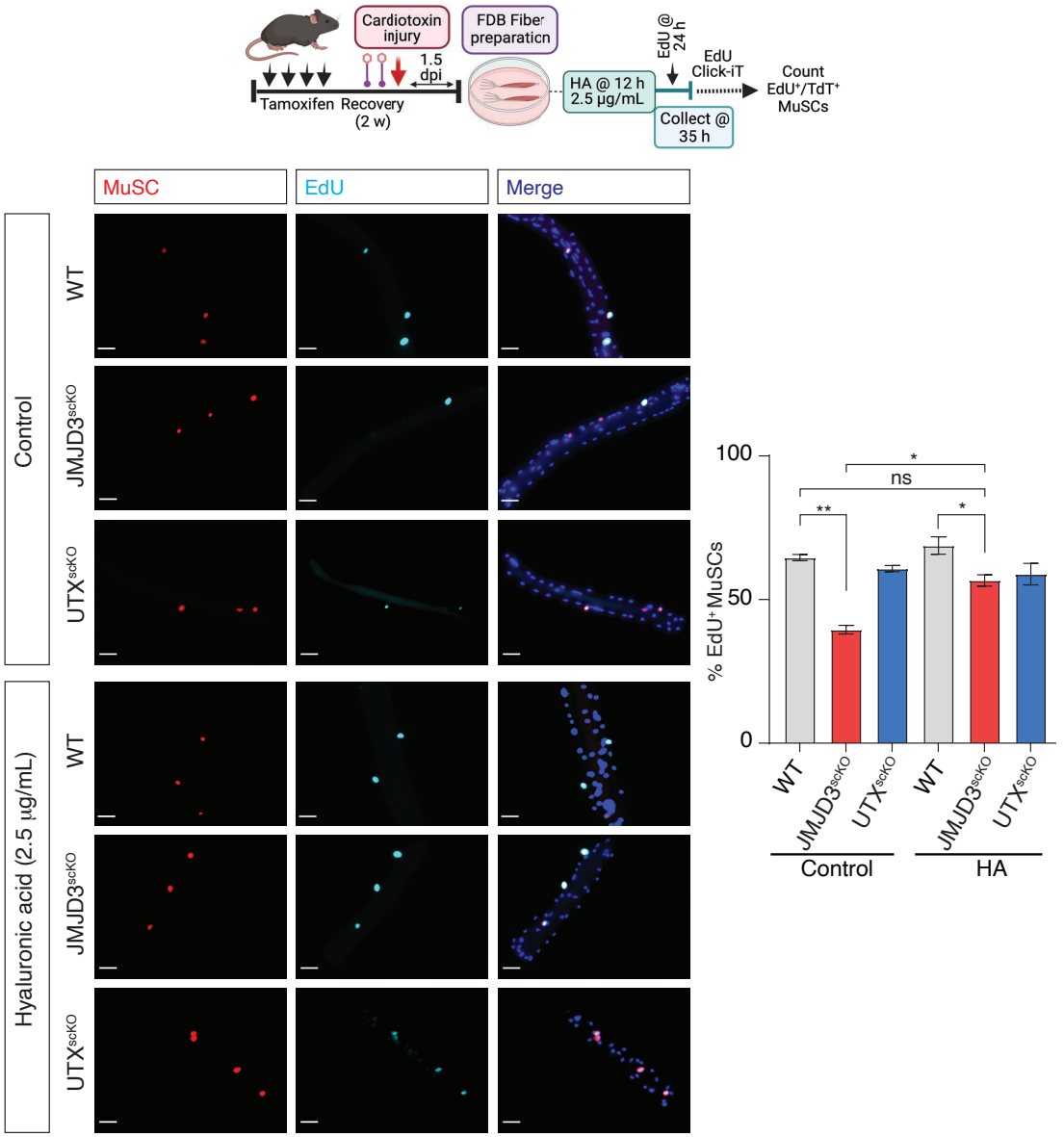


**Fig. S14. Hyaluronic acid rescues the loss of JMJD3 to permit activation of MuSCs.** Quantification of MuSC activation *ex vivo* by immunofluorescence analysis of FDB myofibers (ratio of $TdT^{+}$(Red) and $EdU^{+}$(Cyan)) prepared from indicated mice strains that were previously subjected to injury (CTX injury to contralateral leg 36h prior to FDB myofiber preparation). Myofibers were treated with hyaluronic acid at a concentration of 2.5 µg/mL of media. MuSCs on myofibers prepared from $JMJD3^{scKO}$ mice and treated with HA showed a rescue in delayed activation as evidenced by increased EdU incorporation. Statistical significance was determined using an unpaired *t*-test, ns = not significant, * $p < 0.05$, ** $p < 0.01$, n = >50 fibers for each sample obtained from 3 mice.

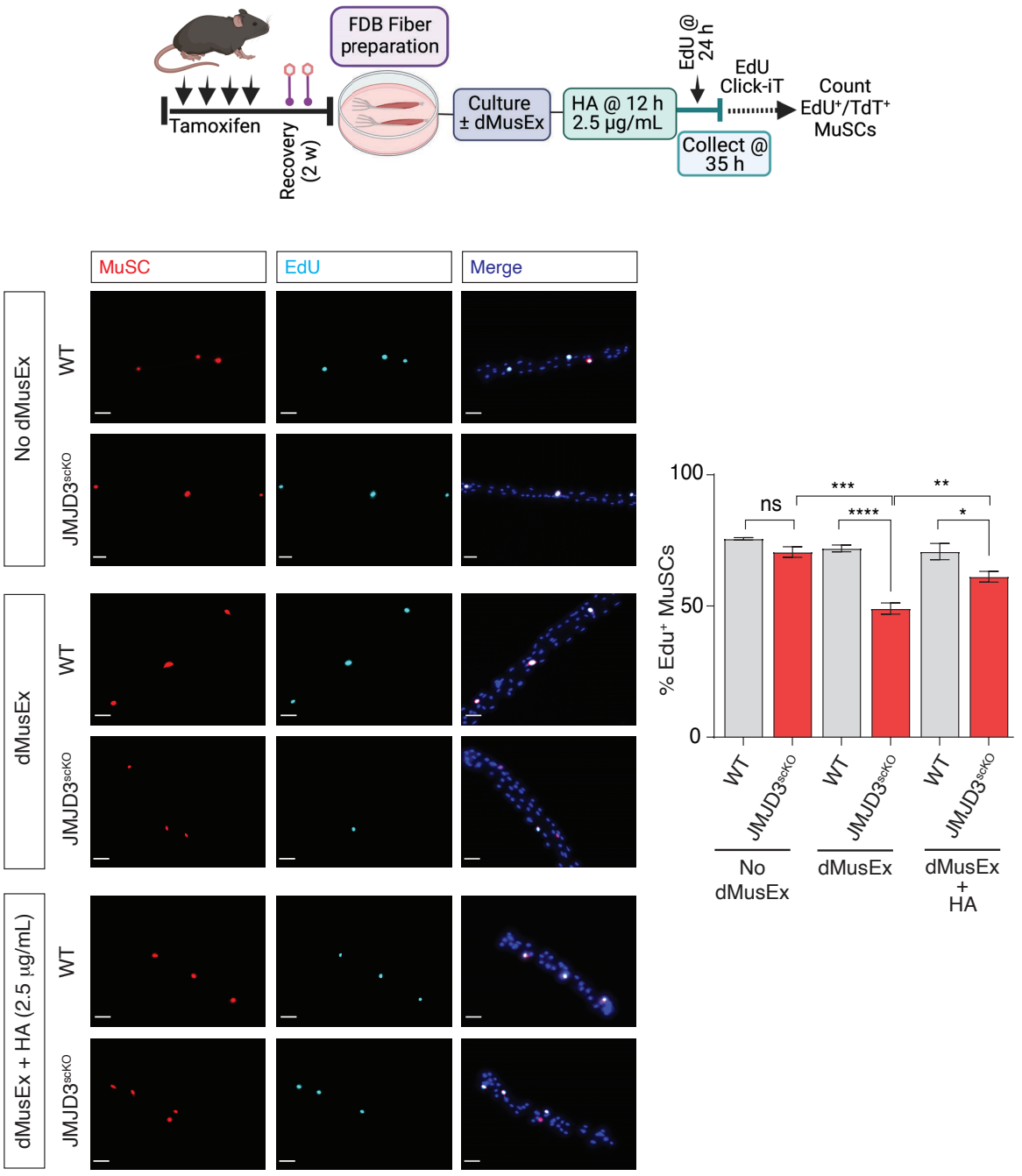


**Fig. S15. Hyaluronic acid rescues activation in JMJD3-null MuSCs treated with dMusEx.** Myofibers were prepared from WT and JMJD3$^{scKO}$ strains of mice that were not subjected to any muscle injury. Myofibers were cultured in the presence or absence of damaged muscle extracts. *ex vivo* MuSC activation was measured by immunofluorescence analysis of FDB myofibers (ratio of TdT$^{+}$(Red) and EdU$^{+}$(Cyan)). Exogenous hyaluronic acid at a concentration of 2.5 µg/mL was supplemented to the culture media of myofibers that were treated with damaged muscle extract. Treatment of myofibers with damaged muscle extract delayed the activation of MuSCs, while

addition of hyaluronic acid rescued the activation of JMJD3$^{scKO}$ MuSCs. Statistical significance was determined using an unpaired *t*-test, ns = not significant, * $p < 0.05$, ** $p < 0.01$, *** $p < 0.001$, ****$p < 0.0001$, n >50 fibers for each sample obtained from 3 mice.

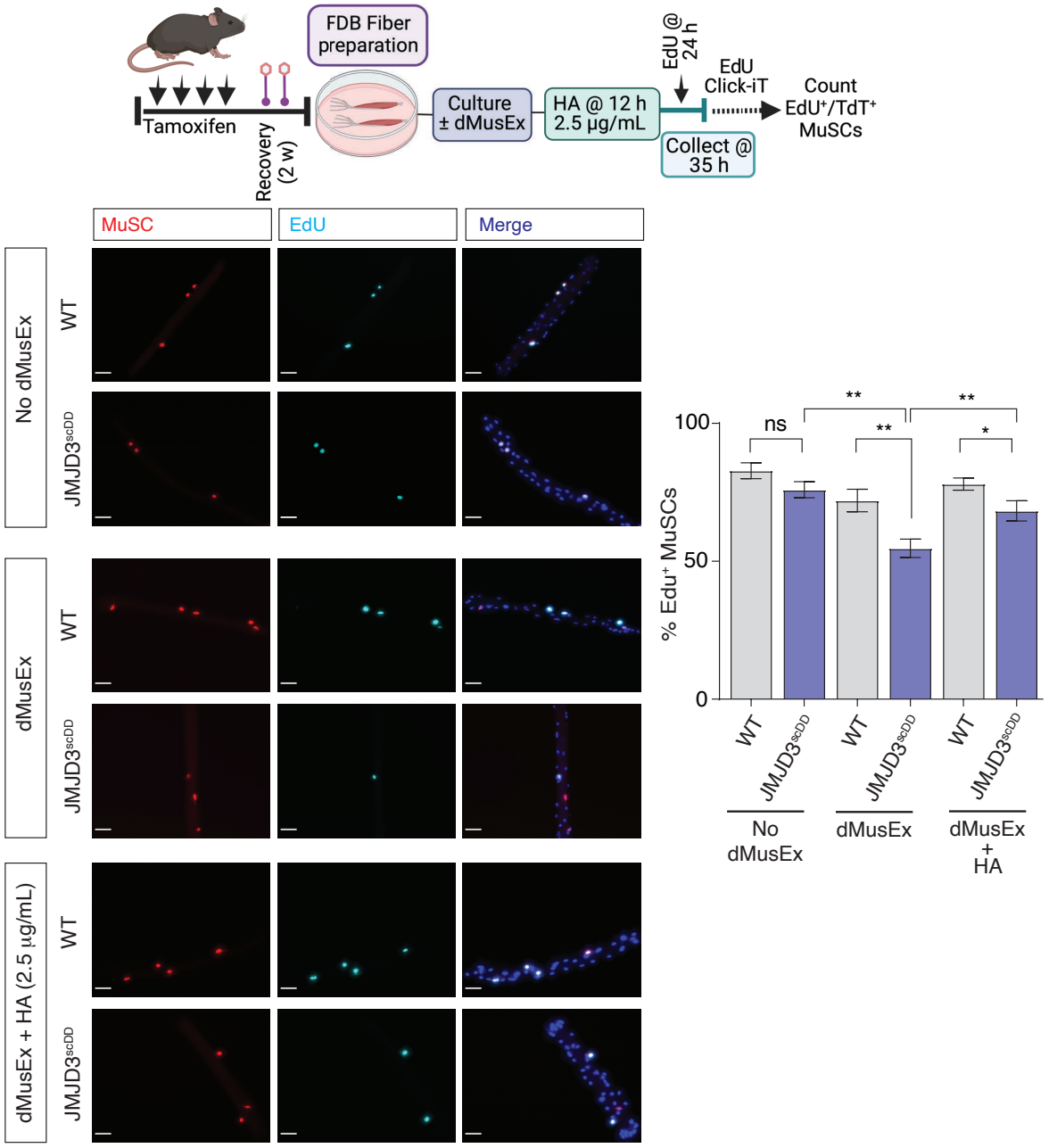


**Fig. S16. Hyaluronic acid rescues activation in JMJD3$^{scDD}$ MuSCs treated with dMusEx.** Myofibers were prepared from WT and JMJD3$^{scDD}$ strains of mice that were not subjected to any muscle injury. Myofibers were cultured in the presence or absence of damaged muscle extracts (dMusEx). *ex vivo* MuSC activation was measured by immunofluorescence analysis of FDB myofibers (ratio of TdT$^{+}$(Red) and EdU$^{+}$(Cyan)). Exogenous hyaluronic acid at a concentration of 2.5 µg/mL was supplemented to the culture media of myofibers that were treated with damaged muscle extract. Treatment of myofibers with damaged muscle extract delayed the activation of

JMJD3$^{scDD}$ MuSCs, while addition of hyaluronic acid rescued the activation. Statistical significance was determined using an unpaired *t*-test, ns = not significant, * $p < 0.05$, ** $p < 0.01$, n = >50 fibers for each sample obtained from 2 mice.

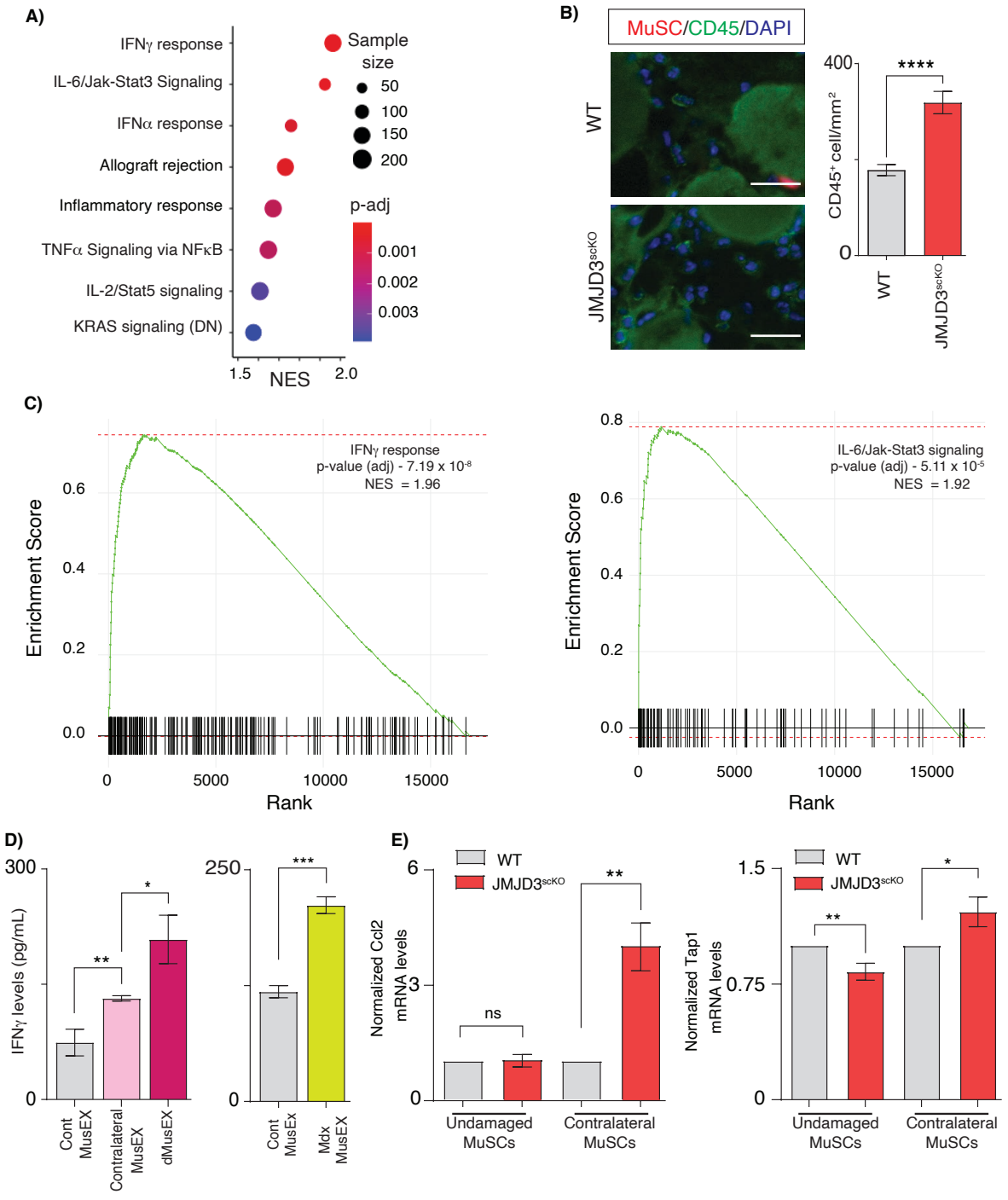


**Fig. S17. The cellular response to pro-inflammatory cytokines is up-regulated in JMJD3$^{scKO}$ MuSCs. A)** Genes that were significantly up-regulated in JMJD3$^{scKO}$ MuSCs showed increased expression of inflammatory response genes by GSEA, with specific enrichment of IFNγ–, TNFα–, and IL6-response genes. **B)** CD45$^{+}$ immune cells accumulate in the regenerating muscle of

JMJD3$^{scKO}$ mice. Cross-sections of injured TA (at 30h post injury) were stained with anti-CD45 antibody (green) to reveal that regenerating muscle from JMJD3$^{scKO}$ mice has significantly more infiltration of immune cells. **C)** GSEA shows a significant enrichment of IFNγ response and IL-6/Jak-Stat3 signaling response genes in JMJD3$^{scKO}$ MuSCs. **D)** Damaged muscle extracts and Mdx muscle extracts show increased presence of IFNγ levels by ELISA, while contralateral muscles have intermediate levels of IFNγ compared to basal levels in control muscle extract. **E)** RT-qPCR analysis of IFNγ response genes - Ccl2 and Tap1, in uninjured and contralateral MuSCs prepared from WT and JMJD3$^{scKO}$ mice. Contralateral JMJD3$^{scKO}$ MuSCs show increased abundance of IFNγ response genes. Statistical significance was determined using an unpaired *t*-test, ns = not significant, * $p<0.05$, ** $p<0.01$, *** $p<0.001$ **** $p<0.0001$, n=3. Scale bar represents 25 μm.

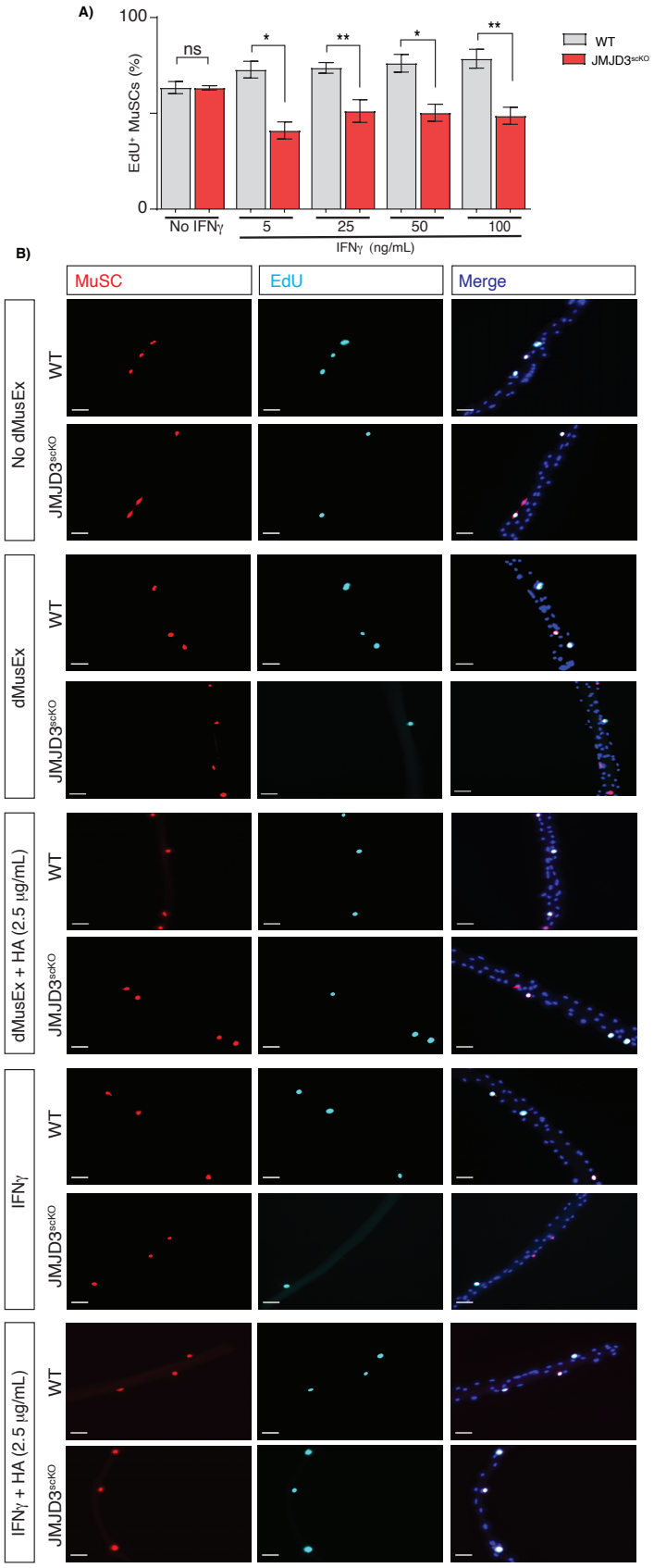
A)
100
0
EdU+ MuSCs (%)
ns
*
**
*
**
WT
JMJD3scKO
No IFNγ
5
25
50
100
IFNγ (ng/mL)
B)
MuSC
EdU
Merge
No dMusEx
dMusEx
dMusEx + HA (2.5 µg/mL)
IFNγ
IFNγ + HA (2.5 µg/mL)
WT
JMJD3scKO

**Fig. S18. Hyaluronic acid treatment can rescue activation of JMJD3$^{scKO}$ MuSCs that have been treated the cytokine IFNγ. A)** IFNγ blocks activation of JMJD3-null MuSCs at a wide range of doses (5 – 100 ng/mL). Myofibers were isolated from FDB muscles of WT and JMJD3$^{scKO}$ mice that were not subjected any muscle injury. Myofiber cultures were treated with indicated amounts of IFNγ. *ex vivo* activation assays were performed to determine at which concentrations the cytokine IFNγ could induce a block to cell cycle re-entry in JMJD3$^{scKO}$ MuSCs. Immunofluorescence analysis measured as percentage of MuSCs (TdT$^{+}$) that were positive for EdU (Cyan), revealed that JMJD3$^{scKO}$ MuSCs show delayed activation in the presence of IFNγ. Statistical significance was determined using an unpaired *t*-test, ns = not significant, * $p<0.05$, ** $p<0.01$, n = >50 fibers for each sample obtained from 2 mice. **B)** Immunofluorescence analysis of MuSCs on FDB myofibers prepared from indicated mouse strains show decreased EdU(cyan) incorporation upon treatment with damaged muscle extract (dMusEx) and 50 ng/mL of IFNγ. Delayed activation of JMJD3$^{scKO}$ MuSCs in both conditions of dMusEx and IFNγ treatment is rescued upon treatment with hyaluronic acid of 2.5 µg/mL of media. Scale bars represent 25 µm.

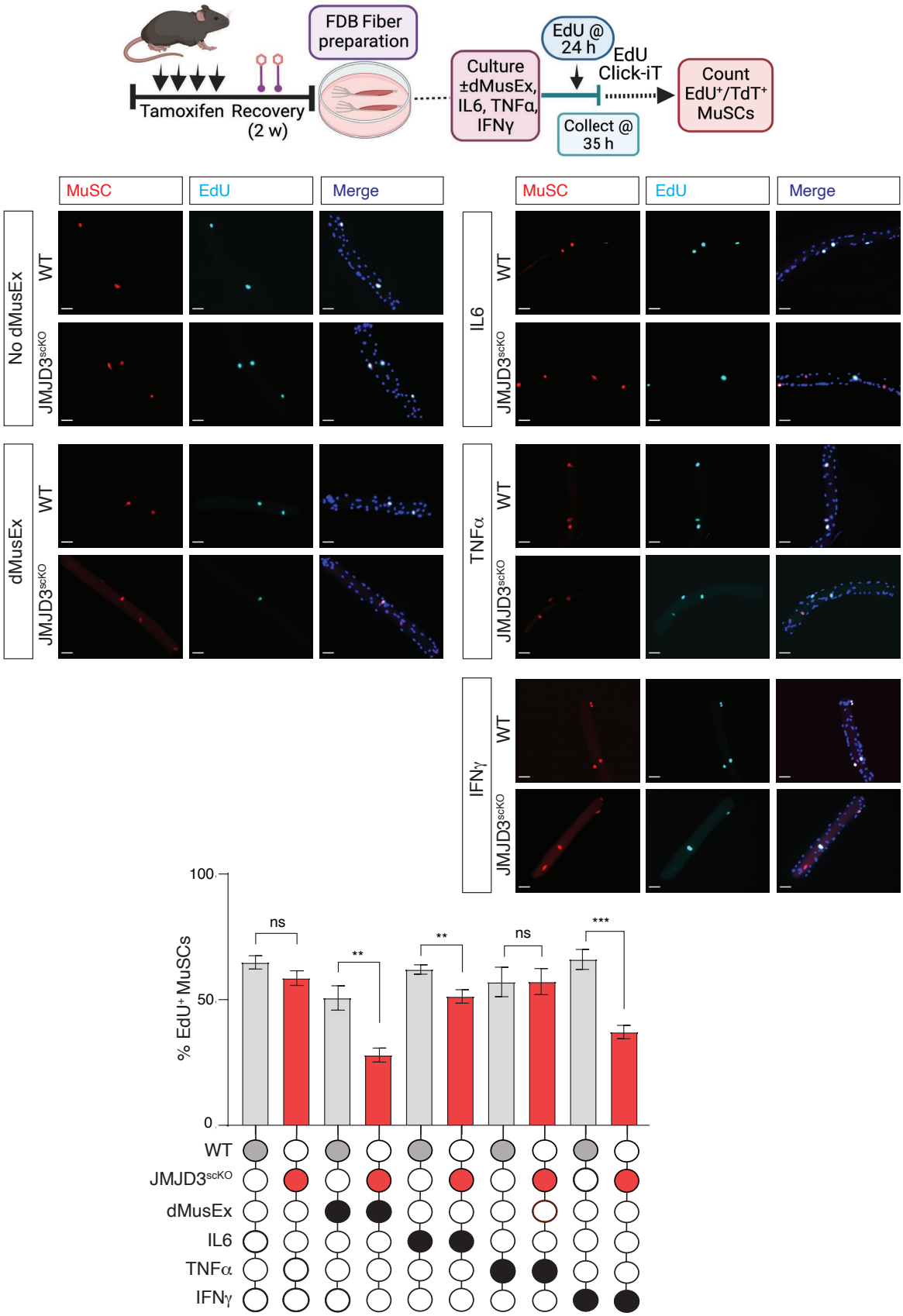
Tamoxifen
Recovery (2 w)
FDB Fiber preparation
Culture ±dMusEx, IL6, TNFα, IFNγ
EdU @ 24 h
EdU Click-iT
Collect @ 35 h
Count EdU+/TdT+ MuSCs
MuSC
EdU
Merge
No dMusEx
dMusEx
IL6
TNFα
IFNγ
WT
JMJD3scKO
% EdU+ MuSCs
100
50
0
ns
**
**
ns
***
WT
JMJD3scKO
dMusEx
IL6
TNFα
IFNγ

**Fig. S19. The pro-inflammatory cytokines IFNγ and IL6 prevent activation of JMJD3-null MuSCs.** Myofibers were prepared from FDB muscle of WT and JMJD3$^{scKO}$ mice. *ex vivo* activation assays were performed to determine which cytokines were contributing to the block in cell cycle re-entry in the absence of JMJD3. Where indicated, myofibers were incubated with either a damaged muscle extract (dMusEx), recombinant IL6, recombinant TNFα or recombinant IFNγ proteins. Immunofluorescence analysis measured percentage of MuSCs (TdT$^{+}$) that were positive for EdU (Cyan). MuSCs obtained from JMJD3$^{scKO}$ show delayed activation with IL6 and IFNγ, but not upon treatment with TNFα. Statistical significance was determined using an unpaired *t*-test, ns = not significant, ** p <0.01, *** p<0.001; n = >50 fibers for each sample obtained from 3 mice. Scale bar represents 25 μm.

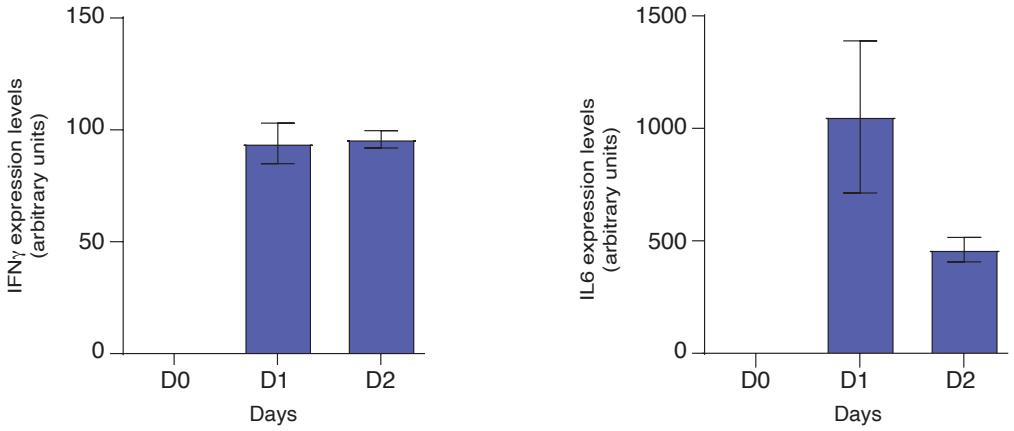


**Fig. S20. Expression of IFNγ and IL-6 in Ly6C$^+$ macrophages present in regenerating muscle**. Re-analysis of published microarray data *(36)* from purified Ly6C$^+$ cells that had been isolated from regenerating muscle showed that IFNγ and IL6 are expressed in regenerating muscle at 24h (D1) and 48h (D2) post CTX-injury. Note that prior to injury (D0), Ly6C$^+$ macrophages were present at insufficient levels in the healthy muscle to allow for purification. Thus, Ly6C$^+$ macrophages infiltrate the regenerating muscle with a kinetic suitable to release IFNγ and IL6 to block MuSC activation.